symmetry

MDPI

Article

Characterization of Spatial Cognitive EEG Signals Using Normalized Adjusted Permutation Conditional Mutual Information

Xianglong Wan [1,2,†], Yue Sun [1,†], Zhenzhen Wu [1,†] and Dong Wen [1,2,*]

[1] School of Intelligence Science and Technology, University of Science and Technology Beijing, Beijing 100083, China
[2] Key Laboratory of Perception and Control of Intelligent Bionic Unmanned Systems, Ministry of Education, Institute of Artificial Intelligence, University of Science and Technology Beijing, Beijing 100083, China
* Correspondence: wencangdong@163.com
† These authors contributed equally to this work.

Abstract: Spatial cognitive ability, a fundamental domain within the human cognitive system, involves the perception, interpretation, and manipulation of spatial environments. This study introduces a new EEG feature extraction algorithm, Normalized Adjusted Permutation Conditional Mutual Information (NAPCMI), to improve the accuracy of spatial cognition assessments. By capturing the symmetry and temporal dependencies within EEG signals during spatial cognition tasks, NAPCMI enhances the ability to extract relevant features. The study validates NAPCMI using a BCI-VR spatial cognition assessment system, incorporating gesture recognition. Results demonstrate that NAPCMI outperforms traditional methods in feature extraction, highlighting its potential for advancing the understanding and assessment of spatial cognitive abilities. The findings also emphasize the significance of specific EEG frequency bands, such as Delta and Beta1, in spatial cognition tasks, further validating NAPCMI's effectiveness.

Keywords: feature extraction from EEG signals; normalized adjusted permutation conditional mutual information; visuospatial cognition; brain-computer interface; virtual reality

Academic Editor: Michel Planat

Received: 4 December 2024
Revised: 23 December 2024
Accepted: 24 December 2024
Published: 17 January 2025

Citation: Wan, X.; Sun, Y.; Wu, Z.; Wen, D. Characterization of Spatial Cognitive EEG Signals Using Normalized Adjusted Permutation Conditional Mutual Information. *Symmetry* **2025**, *17*, 130. https://doi.org/10.3390/sym17010130

1. Introduction

Spatial cognitive ability represents a fundamental domain within the human cognitive system, encompassing the perception, interpretation, and manipulation of spatial environments by individuals [1]. This ability often exhibits symmetrical patterns in brain activity, where specific regions of the brain work in concert to process spatial information [2]. In the fields of medicine, psychology, and human–computer interaction, assessing and training an individual's spatial cognitive abilities is crucial. Traditional methods of assessing spatial cognition have limitations in capturing the complexity and dynamic nature of brain activity during these tasks [3].

To address these limitations, this study introduces a new EEG feature extraction algorithm, Normalized Adjusted Permutation Conditional Mutual Information (NAPCMI) [4]. By incorporating amplitude features, normalization, and permutation-based conditional mutual information, NAPCMI is designed to capture the symmetrical and temporal dependencies within EEG signals during spatial cognition tasks. This approach enhances the algorithm's ability to extract relevant features, providing a more accurate assessment of spatial cognitive abilities.

Training spatial skills are crucial for human cognitive development and functioning as these skills are fundamental to various domains, including navigation, problem-solving, and daily activities. Spatial cognition involves the ability to perceive, interpret, and manipulate spatial relationships, which are essential for tasks such as understanding maps, navigating complex environments, and engaging in spatial reasoning. In individuals with cognitive impairments, deficits in spatial cognition can significantly affect their quality of life, leading to challenges in orientation, memory, and functional independence [5]. For instance, spatial skills are closely linked to spatial memory and visuospatial reasoning, enabling individuals to recognize objects and their relationships in three-dimensional space. Recent advancements in EEG research have highlighted the role of specific brainwave patterns, particularly in the theta and alpha bands, in spatial orientation and memory processes. This underlines the importance of targeted training methods that can enhance these neural pathways. Combining behavioral analyses with EEG signal processing offers a more comprehensive understanding of spatial cognition mechanisms, supporting the development of personalized training and assessment systems.

In recent years, Brain-Computer Interface (BCI) technology combined with virtual reality (VR) environments has enabled richer and more interactive platforms for testing spatial cognition [6]. In VR environments, complex spatial tasks can be simulated to realistically mimic real-world activities, resulting in more precise and sensitive assessment outcomes [7]. However, extracting spatial cognition-related features from complex EEG signals and developing effective algorithms for analysis remain focus areas and challenges in contemporary research [8].

Feature extraction of EEG signals is a pivotal step in spatial cognition assessment [9]. Traditional methods, such as Spectral Analysis [10,11] and Wavelet Transform [12,13], demonstrate limited effectiveness, often overlooking the temporal and multidimensional coupling features of EEG signals [14]. Information theory-based methods, such as Permutation Conditional Mutual Information (PCMI), have been introduced to analyze coupling features, revealing patterns of information exchange between brain regions [15]. However, PCMI approaches primarily emphasize the temporal structure of signals while neglecting amplitude features, limiting the expressiveness of extracted features.

To address these limitations, researchers have proposed improved PCMI-based algorithms, including Normalized Permutation Conditional Mutual Information (NPCMI) [16], Multivariate Permutation Conditional Mutual Information (MPCMI) [17], and Adjusted Permutation Conditional Mutual Information (APCMI) [18]. NPCMI improves feature stability through normalization, MPCMI enhances spatial coupling resolution with multidimensional connectivity metrics, and APCMI employs a weighting strategy to increase feature sensitivity. Building on these advancements, this study introduces a new EEG feature extraction method: Normalized Adjusted Permutation Conditional Mutual Information (NAPCMI). By integrating amplitude features and normalization into the PCMI framework, NAPCMI improves algorithm robustness and generalization.

To validate NAPCMI, this study designs and develops a spatial cognitive assessment system based on BCI-VR. The system incorporates a desktop computer, HTC VIVE head-mounted device, Leap Motion Controller gesture recognizer, and OpenBCI EEG signal acquisition device. It enables participants to engage in spatial cognition tasks within a VR environment while simultaneously collecting EEG data in real-time. The experimental design includes the complete workflow from pattern memorization to reconstruction, facilitating the analysis of alterations in EEG features pre- and post-task. The results indicate that NAPCMI outperforms NPCMI, MPCMI, and APCMI in feature extraction across different frequency band combinations, introducing a novel analytical approach for spatial cognitive ability assessment.

2. Methods

The proposed NAPCMI algorithm calculates the coupled features based on weighted permutation conditional mutual information, considering the amplitude and normalization of EEG signals. By permutation, the algorithm can capture the temporal dependencies and symmetrical patterns within EEG signals during spatial cognition tasks. This approach allows for a more comprehensive feature extraction, enhancing the accuracy of spatial cognition assessments.

MPCMI incorporates the influence of adjacent brain regions into the PCMI framework, thereby enhancing the precision of coupling feature extraction. Building upon these approaches, this paper enhances the traditional EEG coupling feature extraction method and proposes a feature extraction approach based on normalized adjusted permutation conditional mutual information, where the amplitude features of the EEG signal are integrated with sequential structural features using a weighted formulation. This improvement achieves higher accuracy in EEG connectivity estimation.

Figure 1 illustrates the NAPCMI feature extraction workflow for EEG signals, as outlined in this chapter.

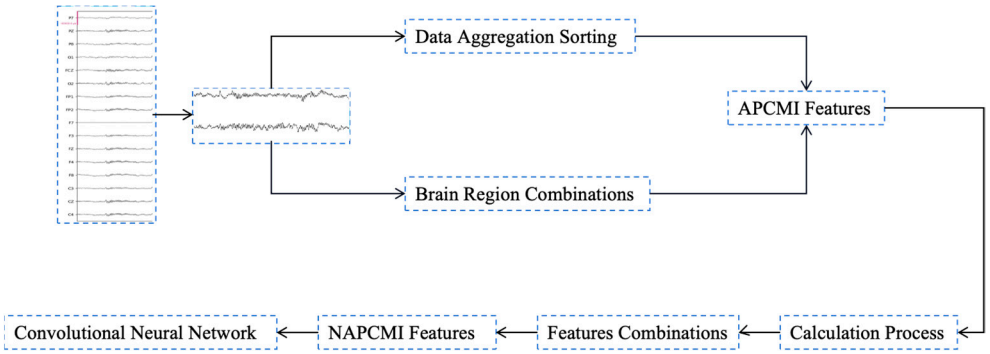

Figure 1. NAPCMI feature extraction flowchart.

2.1. Detailed Description of the Algorithm

The computational process of the NAPCMI feature extraction method is divided into three main steps:

Permuting EEG Signals: The experimentally acquired EEG signals are permuted according to predefined patterns. For each permutation pattern, the standard deviations of the corresponding signal series are computed. The standard deviations for the same permutation patterns across different brain regions are multiplied to obtain weighted values for the combinations of these regions.

Calculating Coupling Features: The coupling feature values between different brain regions are derived using the permuted conditional mutual information approach. These values incorporate the weighted standard deviations from the previous step to enhance the representation of inter-regional interactions.

Normalization of Connectivity Metrics: The connectivity metrics obtained from the weighted permutation conditional mutual information are normalized. This process involves applying the standard deviations computed earlier to weight the conditional mutual information under each permutation pattern, ensuring consistency and robustness.

The algorithm's specific steps for extracting normalized weighted conditional mutual information are detailed below.

2.1.1. Calculation of Weights Based on Standard Deviation

Two-time series X and Y, denoted as $X = (x_1, \ldots, x_n)^T$ and $Y = (y_1, \ldots, y_n)^T$, respectively, are arbitrarily selected, where n is the number of EEG signal observation points.

Embedding them into the m-dimensional space and selecting one data point every τ time interval, $(n-(m-1)\tau)$ m-dimensional space vectors X_i and Y_j can be obtained, where X_i is denoted as $X_i = \left(x_i, x_{i+\tau}, \ldots, x_{i+(m-1)\tau}\right)^T, i = 1, \ldots, n-(m-1)\tau$, and Y_j is denoted as $Y_j = \left(y_i, y_{j+\tau}, \ldots, y_{j+(m-1)\tau}\right)^T, j = 1, \ldots, n-(m-1)\tau$.

Then the elements in the m dimensional spatial vectors in the two brain region sequences X_i and Y_j are permuted in ascending order, respectively, and when the values of the elements in them are equal in magnitude, they are permuted according to the value of the subscript of the element (i or j), and therefore, $m!$ different permutation patterns can be obtained according to the permutation pattern, which are denoted as π_{x_i}, $i = 1, \ldots, m!$ and π_{y_j}, $j = 1, \ldots, m!$, where π_{x_i} and π_{y_j} denote the i and j permutation under the X and Y brain regions, respectively. Furthermore, the vectors with the same permutation pattern are combined into the same sequence, which is denoted as S_{x_i}, $i = 1, \ldots, m!$ and S_{y_j}, $j = 1, \ldots, m!$, where S_{x_i} denotes $S_{x_i} = \{s_{x_1}, \ldots, s_{x_t}\}$, S_{y_j} denotes $S_{y_j} = \{s_{y_1}, \ldots, s_{y_t}\}$, and t is the number of vectors, and the number of vectors in the sequences of S_{x_i} and S_{y_j} under $m!$ different permutation patterns are different. Finally, the standard deviation of the sequences of S_{x_i} and S_{y_j} under $m!$ different permutation modes is calculated, respectively, which are denoted as W_{x_i}, $i = 1, \ldots, m!$ and W_{y_j}, $j = 1, \ldots, m!$. The formulas for calculating W_{x_i} and W_{y_j} are shown in Equations (1) and (2):

$$W_{x_i} = \sqrt{\frac{\sum_{t}^{z=1} \left(s_{x_i} - \overline{s_{x_i}}\right)^2}{t}}, \; i = 1, \ldots, m!, \tag{1}$$

$$W_{y_j} = \sqrt{\frac{\sum_{t}^{z=1} \left(s_{y_j} - \overline{s_{y_j}}\right)^2}{t}}, \; j = 1, \ldots, m!, \tag{2}$$

2.1.2. Calculation of Coupled Features Based on Weighted Permutation Conditional Mutual Information

After the standard deviation of EEG amplitude of different permutation modes of X_{x_i} and Y_{y_j} sequence obtained by the above calculation, this paper multiplies the standard deviation of EEG amplitude under the same permutation modes to obtain and then uses $W_{x_i} \times W_{y_j}$ to weight the entropy of the permutation conditions under the corresponding permutation modes to incorporate the amplitude features of EEG signals into the connectivity metrics of the permutation conditions mutual information.

Based on the permutation results of the two spatial vectors X_i and Y_j in the previous subsection, this paper calculates the number of times that each permutation pattern appears under the X and Y brain regions, which are denoted as C_{x_i}, $i = 1, \ldots m!$ and C_{y_j}, $j = 1, \ldots m!$, respectively, and from this, the probability of the appearance of each permutation pattern under the brain regions $P(x_i)$, $i = 1, \ldots, m!$ can be calculated, as shown in Equation (3).

$$P(x_i) = P(\pi_{x_i}) = \frac{C_{x_i}}{(n-(m-1)\tau)}, \; i = 1, \ldots, m!, \tag{3}$$

Similarly, the probability of occurrence of each permutation pattern under Y brain regions can be calculated as $P\left(y_j\right)$, $j = 1, \ldots, m!$, which is shown in Equation (4):

$$P\left(y_j\right) = P\left(\pi_{y_j}\right) = \frac{C_{y_j}}{(n-(m-1)\tau)}, \; j = 1, \ldots, m!, \tag{4}$$

According to the above analysis, it can be seen that there are a total of $m! \times m!$ kinds of joint permutation patterns in X and Y two brain regions under the same moment, and in this paper, the number of times each joint permutation pattern appeared is calculated to record $C_{x_i y_j},\ i,j = 1,\ldots m!$. From this, the probability of the appearance of each joint permutation pattern can be calculated to be $P(x_i, y_j),\ i,j = 1,\ldots,m!$, and its calculation formula is shown in Equation (5):

$$P(x_i, y_j) = P\left(\pi_{x_i}, \pi_{y_j}\right) = \frac{C_{x_i y_j}}{(n-(m-1)\tau)},\ i,j = 1,\ldots,m!, \tag{5}$$

Similarly, the probability of the appearance of the permutation pattern in brain region X under the condition that the permutation pattern exists in brain region Y at the same moment can be calculated as $P(x_i|y_j),\ i,j = 1,\ldots,m!$, which is shown in Equation (6):

$$P(x_i|y_j) = P\left(\pi_{x_i}\middle|\pi_{y_j}\right) = \frac{C_{\frac{x_i}{y_j}}}{(n-(m-1)\tau)},\ i,j = 1,\ldots,m!, \tag{6}$$

For the convenience of calculation in this paper, the probability of occurrence of the permutation pattern under X and Y brain regions and the joint probability and conditional probability of the two is denoted as $P(X),\ P(Y),\ P(X,Y),\ P(X|Y)$ and $P(Y|X)$, respectively, according to which the permutation entropy $PE(X)$ and $PE(Y)$, the permutation joint entropy $PE(X,Y)$, and the permutation conditional entropy $PE(X|Y)$ and $PE(Y|X)$ of the permutation pattern under X and Y brain regions can be calculated, and the formulas thereof are as shown in the formulae Equations (7)–(11):

$$PE(X) = -\sum_{m!}^{i=1} P(x_i) log(P(x_i)), \tag{7}$$

$$PE(Y) = -\sum_{m!}^{j=1} P(y_j) log(P(y_j)), \tag{8}$$

$$PE(X,Y) = -\sum_{m!}^{i=1}\sum_{m!}^{j=1} P(x_i, y_j) log(P(x_i, y_j)), \tag{9}$$

$$PE(X|Y) = -\sum_{m!}^{i=1}\sum_{m!}^{j=1} P(x_i, y_j) log(P(x_i|y_j)), \tag{10}$$

$$PE(Y|X) = -\sum_{m!}^{i=1}\sum_{m!}^{j=1} P(x_i, y_j) log(P(y_j|x_i)), \tag{11}$$

From the above formula, we can obtain the formula for the permutation conditional mutual trust between the two brain regions X and Y as shown in Equation (12):

$$PMI(X;Y) = PE(X) + PE(Y) - PE(X,Y), \tag{12}$$

The weights W_{x_i} and W_{y_j} of X and Y brain regions in different permutation modes are obtained by using the calculations in the previous subsection, which are applied to the several permutation entropies mentioned above in a multiplicative manner and are calculated to obtain the weighted permutation entropies $APE(X)$ and $APE(Y)$, weighted permutation joint entropy $APE(X,Y)$, weighted permutation conditional entropy $APE(X|Y)$ and $APE(Y|X)$, whose calculations are shown in Equations (13)–(17):

$$APE(X) = -\sum_{m!}^{i=1} W_{x_i} P(x_i) log(P(x_i)), \tag{13}$$

$$APE(Y) = -\sum_{m!}^{j=1} W_{x_i} P(y_j) log\big(P(y_j)\big), \tag{14}$$

$$APE(X,Y) = -\sum_{m!}^{i=1}\sum_{m!}^{j=1} W_{x_i} W_{y_j} P(x_i,y_j) log\big(P(x_i,y_j)\big), \tag{15}$$

$$APE(X|Y) = -\sum_{m!}^{i=1}\sum_{m!}^{j=1} W_{x_i} W_{y_j} P(x_i,y_j) log\big(P(x_i|y_j)\big), \tag{16}$$

$$APE(Y|X) = -\sum_{m!}^{i=1}\sum_{m!}^{j=1} W_{x_i} W_{y_j} P(x_i,y_j) log\big(P(y_j|x_i)\big), \tag{17}$$

From the above formula, the formula for the adjusted permutation conditional mutual trust between the two brain regions X and Y can be obtained, as shown in Equation (18).

$$APMI(X;Y) = APE(X) + APE(Y) - APE(X,Y), \tag{18}$$

In this paper, X_δ and Y_δ are defined as the EEG signals after the delay time δ of X and Y EEG signals, respectively (where the value of δ ranges from 3 to 15), i.e., $\delta = 1,\ldots,15$, and the m-dimensional space vectors of X_δ and Y_δ are denoted as $X_k = \Big(x_k, x_{k+\tau},\ldots,x_{k+(m-1)\tau}\Big)^T$, $k = i+\delta$ and $Y_k = \Big(y_k, y_{k+\tau},\ldots,y_{k+(m-1)\tau}\Big)^T$, $k = i+\delta$. In order to analyze the effects of the EEG signals on the future X and Y moments in the existence of X and Y two EEG signals, the joint probability and conditional probability X_δ and Y_δ for $X,\ Y,\ X_\delta$ and $X,\ Y,\ Y_\delta$ under different ordering modes (there are $m!\times m!\times m!\times m!$ ordering modes) under the joint probability and conditional probability $P(X,Y,X_\delta),\ P(X,Y,Y_\delta),\ P(Y,X_\delta|X)$ and $P(X,Y_\delta|Y)$. From this, the weighted sequencing joint entropy $X,\ Y,\ X_\delta$ as well as $X,\ Y,\ Y_\delta$ and the weighted sequencing conditional entropy $APE(X,Y,X_\delta)$ as well as $APE(X,Y,Y_\delta)$ of the joint EEG sequences of $APE(Y,X_\delta|X)$ and $APE(X,Y_\delta|Y)$ can be computed, which are shown in the formulas of Equations (19)–(22):

$$APE(X,Y,X_\delta) = -\sum_{m!}^{i=1}\sum_{m!}^{j=1}\sum_{m!}^{k=1} W_{x_i} W_{y_j} W_{x_{\delta k}} P(x_i,y_j,x_k) log\big(P(x_i,y_j,x_k)\big), \tag{19}$$

$$APE(X,Y,Y_\delta) = -\sum_{m!}^{i=1}\sum_{m!}^{j=1}\sum_{m!}^{k=1} W_{x_i} W_{y_j} W_{y_{\delta k}} P(x_i,y_j,y_k) log\big(P(x_i,y_j,y_k)\big), \tag{20}$$

$$APE(Y,X_\delta|X) = -\sum_{m!}^{i=1}\sum_{m!}^{j=1}\sum_{m!}^{k=1} W_{x_i} W_{y_j} W_{x_{\delta k}} P(x_i,y_j,x_k) log\big(P(y_j,x_k|x_i)\big), \tag{21}$$

$$APE(X,Y_\delta|Y) = -\sum_{m!}^{i=1}\sum_{m!}^{j=1}\sum_{m!}^{k=1} W_{x_i} W_{y_j} W_{y_{\delta k}} P(x_i,y_j,y_k) log\big(P(x_i,y_k|y_j)\big), \tag{22}$$

Based on the above results, it is possible to calculate the effect of the EEG sequence Y on the amount of information in the X_δ sequence at δ delayed X moments, weighted permutation conditional mutual information $APCMI^\delta_{Y\to X}$, and the effect of the EEG sequence Y on the amount of information in the Y_δ sequence at δ delayed X moments, weighted ordering conditional mutual information $APCMI^\delta_{X\to Y}$, which is calculated as shown in Equations (23) and (24):

$$APCMI^\delta_{Y\to X} = APE(Y;X_\delta|X) = APE(Y|X) + APE(X_\delta|X) - APE(Y,X_\delta|X), \tag{23}$$

$$APCMI^\delta_{X\to Y} = APE(X;Y_\delta|Y) = APE(X|Y) + APE(Y_\delta|Y) - APE(X,Y_\delta|Y) \tag{24}$$

2.1.3. Normalisation Based on Mutual Information

This paper calculates the normalized adjusted permutation conditional mutual information of X and Y EEG signals by normalizing the adjusted permutation conditional mutual information obtained above according to the method of normalized mutual information.

The formula for the normalized mutual information $NMI(X;Y)$ is shown in Equation (25):

$$NMI(X;Y) = \frac{2I(X;Y)}{H(X) + H(Y)}, \tag{25}$$

Similarly, the normalized adjusted permutation conditional mutual information X and Y of the EEG signals of $NAPCMI^{\delta}_{Y\to X}$ and $NAPCMI^{\delta}_{X\to Y}$ can be calculated according to the above formulae, as shown in Equations (26) and (27):

$$NAPCMI^{\delta}_{Y\to X} = \frac{2APCMI^{\delta}_{Y\to X}}{APE(Y|X) + APE(X_{\delta}|X)}, \tag{26}$$

$$NAPCMI^{\delta}_{X\to Y} = \frac{2APCMI^{\delta}_{X\to Y}}{APE(X|Y) + APE(Y_{\delta}|Y)}, \tag{27}$$

Finally, based on the above calculation method, the normalized weighted permuted conditional mutual information of X and Y EEG signals at different delay moments δ is sequentially calculated in this paper to derive the coupling strengths $NAPCMI_{Y\to X}$ and $NAPCMI_{X\to Y}$ between X and Y EEG signals, which are shown in Equations (28) and (29):

$$NAPCMI_{Y\to X} = \frac{1}{N}\sum^{\delta=3}_{N} NAPCMI^{\delta}_{Y\to X}, \tag{28}$$

$$NAPCMI_{X\to Y} = \frac{1}{N}\sum^{\delta=3}_{N} NAPCMI^{\delta}_{X\to Y}, \tag{29}$$

where N is the maximum value of the time delay X that can be selected, and in this paper the maximum value of X is set to 15.

2.2. Sequential Backward Selection of Optimal EEG Feature Band Combinations

Since the EEG feature signals analyzed in this study span seven frequency bands, we investigate the relationship between spatial cognitive ability and EEG features across these frequency bands and identify the optimal combination of frequency bands. To achieve this, the Sequential Backward Selection (SBS) method, a heuristic search approach that iteratively removes one feature dimension per round, is employed to determine the optimal frequency band combination using the sklearn estimator.

Previously, Wu et al. [19] applied the SBS method to select optimal subsets of EEG features, including band power and correlation coefficients, effectively distinguishing between patients with severe depression and healthy individuals. The detailed workflow of the SBS process employed in this study is depicted in Figure 2. Firstly, the feature extraction algorithm is applied to derive connectivity metrics across C frequency bands of the EEG signal. The resulting connectivity metrics, structured as feature data of size K × K × C, are then input into the SBS model. Using a traversal method, one EEG feature dimension is removed in each iteration. The sklearn estimator, based on a classical CNN algorithm, evaluates the performance of different frequency band combinations, with test accuracy used as the evaluation metric. Finally, the optimal combination of EEG frequency bands is identified based on the evaluation scores.

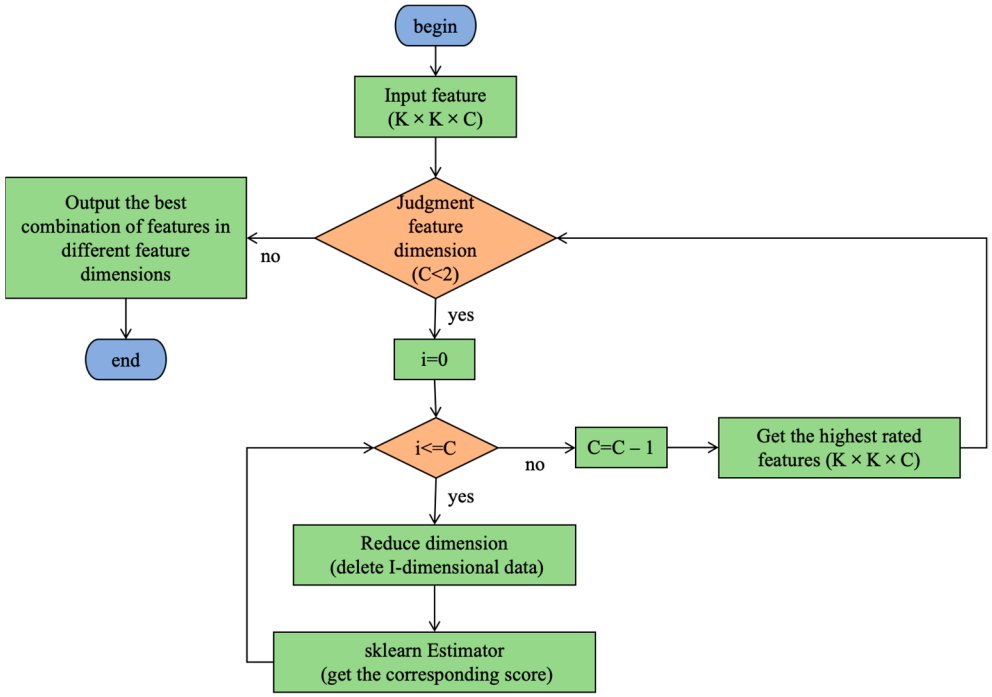

Figure 2. Flowchart of the sequential backward selection process.

2.3. Classification of EEG Signals

The structural framework of convolutional neural networks (CNN) is utilized, and a CNN is designed to accommodate the EEG coupling feature NAPCMI introduced in this chapter, with its network architecture illustrated in Figure 3.

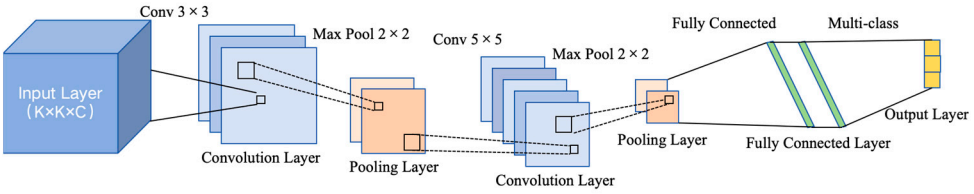

Figure 3. Architecture of the CNN.

Firstly, the NAPCMI EEG feature extraction method proposed in this chapter is used to compute connectivity metrics across seven frequency bands: Delta (1–4 Hz), Theta (4–8 Hz), Alpha1 (8–10.5 Hz), Alpha2 (10.5–13 Hz), Beta1 (13–20 Hz), Beta2 (20–30 Hz), and Gamma (30–40 Hz). The selected connectivity metrics are fused into a three-dimensional feature matrix, which is then input into a CNN for classification and identification.

The input layer accepts input data of size K × K × C, where K = 16, and C represents the number of selected frequency bands. The first convolutional layer consists of 64 convolutional kernels, each with a size of 3 × 3 and a stride of 1. This layer extracts important features, and the Rectified Linear Unit (ReLU) activation function is applied to address the gradient vanishing problem. The first pooling layer applies max pooling with a kernel size of 2 × 2 and a stride of 2, reducing the dimensionality of the feature matrix.

The second convolutional layer uses 32 convolutional kernels, each with a size of 5 × 5 and a stride of 1, to extract further features. This is followed by the second pooling layer, which again employs max pooling with a kernel size of 2 × 2 and a stride of 2 to further reduce the dimensionality of the feature matrix. The flattened layer then flattens the feature matrix into a one-dimensional vector.

The fully connected layer contains 1024 nodes, re-fitting the features and minimizing feature loss. Finally, the output layer performs binary classification using a fully connected structure and applies the Softmax activation function to estimate probabilities.

All algorithms in this study were implemented in Python, utilizing TensorFlow and Keras frameworks for model development and execution.

3. Experimental Design and Methodology

3.1. Development of the Experimental System

The BCI-VR spatial cognition assessment system incorporates gesture recognition and is designed to evaluate symmetrical patterns in brain activity during spatial cognition tasks. Participants perform spatial memory reconstruction tasks within a VR environment, while their EEG signals are collected in real-time. The system enables the analysis of symmetrical patterns in brain activity related to spatial cognition, facilitating the validation of the proposed NAPCMI algorithm.

The desktop computer is equipped with an Intel i5-10400F processor, NVIDIA RTX 2060 graphics card, 16 GB DDR4 RAM, and 1 TB SSD storage, and runs on Windows 10. It serves as the platform for loading and running the cognitive assessment system software. The HTC VIVE headset is used to present VR scenes for spatial cognitive assessment tasks and employs a spatial locator to track the positions of participants. The Leap Motion Controller enables hand gesture control in the VR environment by using a binocular camera to capture hand movements. The parameters of hand tracking are analyzed and integrated into the VR scene, allowing users to manipulate virtual hands. The OpenBCI EEG signal acquisition device collects EEG signals at a sampling rate of 1000 Hz with impedance levels below 10 kΩ. The collected EEG signals are transmitted wirelessly to the computer via Wi-Fi.

3.2. Experimental Design Methodology

The BCI-VR spatial cognition evaluation system with integrated gesture recognition, designed in this study, operates in three main stages: preparation, task execution, and data analysis.

Preparation Stage: The HTC VIVE headset and Leap Motion gesture recognizer are connected to the computer. The spatial locator is calibrated through Steam VR, and the connection between Leap Motion and the computer is verified using the Leap Motion Control Panel to ensure proper functionality. The OpenBCI EEG signal acquisition device is then powered on and connected to the computer's LAN via Wi-Fi. EEG signal quality is checked using OpenGUI to ensure reliable data transmission.

Task Execution Stage: Once all hardware devices are operational, the subject performs the spatial cognitive assessment task as instructed. The subjects complete a total of 28 tasks during the experimental period. This includes tasks from both the pre- and post-training assessments as well as the 28-day spatial cognitive training, which are designed to comprehensively evaluate spatial cognition. The number of tasks is based on the need to assess changes in cognitive ability before and after the training period, ensuring that the data captured provides a reliable and valid measurement of improvement. The VR scene is projected onto the computer screen for real-time monitoring and debugging by the experimenters, who also record behavioral data. Simultaneously, the subject's EEG signals are received and stored in synchronization with the task.

Data Analysis Stage: After completing the task, the behavioral and EEG data are systematically analyzed. The spatial cognitive ability of the subject is evaluated based on the analysis results.

3.2.1. Design and Implementation of a Virtual Spatial Memory Reconstruction Task

This study employs the Unity 3D game development platform to design memory patterns for the memory stage, as illustrated in Figure 4. The patterns are constructed using three basic blue blocks: squares, rectangles, and polyhedra. The overall design consists of four mini-patterns—rectangles, triangles, trapezoids, and I-zigzag shapes. Yellow segments are added to distinguish the positions of the four mini-patterns, each comprising six blocks, resulting in a total of 24 blocks in the complete pattern.

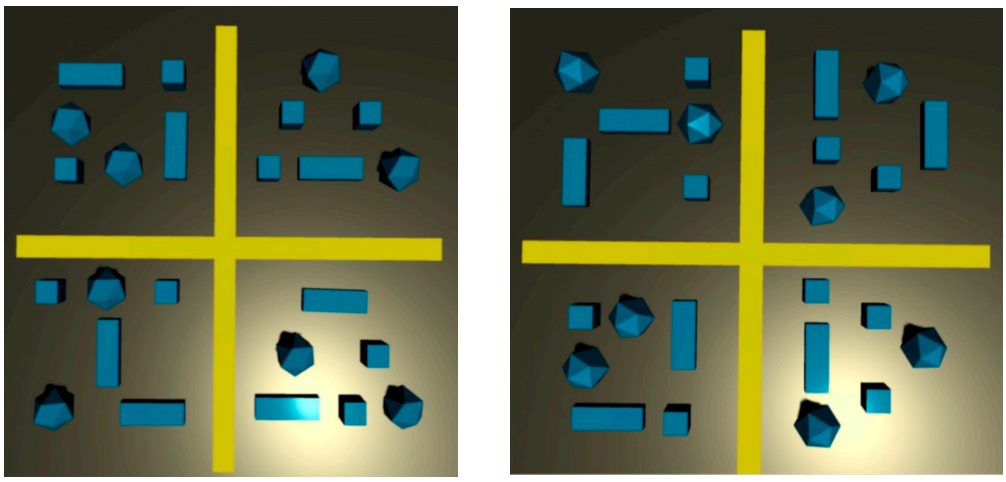

(**a**) (**b**)

Figure 4. Memory Pattern: (**a**) Baseline memory pattern; (**b**) Post-training memory patterns.

Two memory patterns were used in the assessment task. Participants memorized pattern (a) (Figure 4) before training and pattern (b) (Figure 4) after training. To ensure consistent difficulty between pre-training and post-training memory patterns, the four mini-patterns in pattern (b) were positionally transformed and rotated 90 degrees clockwise. The memory patterns are depicted in Figure 4.

The scoring rules for the game are as follows:

General Shape Patterns: Correct placement of each of the four small patterns earns 0.5 points, with a maximum of 2 points.

Pattern Positions: Correct placement of each of the four small patterns in their designated positions earns 0.5 points, with a maximum of 2 points.

Block Locations: Correct placement of each of the 24 small blocks earns 0.5 points, with a maximum of 12 points.

The total score for the game is 16 points.

3.2.2. Design of Assessment Tasks

In the Spatial Memory Pattern Reconstruction Game task, participants memorized a specific pattern as per the experimental requirements. After a set memorization period, they entered the VR spatial scene using the HTC VIVE headset to reconstruct the pattern within a specified time limit. Scoring was based on the accuracy of the pattern's shape and location. The assessment task consisted of three stages: familiarization with the game, pattern memorization, and pattern reconstruction.

Familiarization Stage: As participants were initially unfamiliar with the HTC VIVE headset and Leap Motion gesture recognizer, this could affect the assessment of spatial cognitive ability. To address this, participants first entered the VR space and performed guided familiarization tasks until they were fully comfortable with the equipment and controls.

Pattern Memorization Stage: After familiarization, participants were given 3 min to memorize a specific pattern. The pattern was constructed using 24 blocks, categorized into

3 basic shapes: squares, rectangles, and polyhedra. Every 6 blocks formed a small pattern, and 4 small patterns combined to create the overall pattern.

Pattern Reconstruction Stage: Following the 3-min memorization period, participants donned the VR equipment and entered the game space to reproduce the memorized pattern using the 3 basic blocks. The reconstruction task had an 8-min time limit, during which the completion time and accuracy score were recorded.

3.3. Experimental Analysis Methods

In this study, the spatial cognitive ability of participants was assessed by combining behavioral data and EEG signal analysis before and after training, as illustrated in Figure 5.

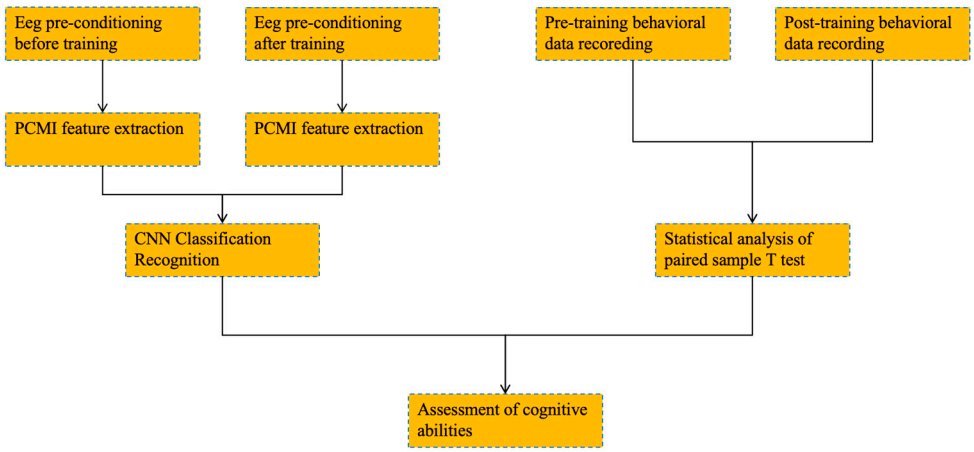

Figure 5. Schematic block diagram of the spatial cognition assessment framework.

For EEG signals, data from cognitive assessment tasks performed before and after training were analyzed. Connectivity metrics were extracted using the permuted conditional mutual information method and classified using CNN to evaluate changes in spatial cognitive ability.

For behavioral data, task completion time and scores from cognitive assessment tasks were analyzed using a paired-sample *t*-test to compare performance before and after training.

Finally, the results from EEG signal analysis and behavioral data were integrated to systematically evaluate the spatial cognitive ability of participants.

In this study, a paired-sample *t*-test was conducted to evaluate differences in performance on the spatial cognition assessment task before and after training. This statistical method is commonly used to compare the same individuals under different conditions or time points by analyzing the mean and standard deviation of paired differences.

In this experiment, the paired-sample *t*-test was applied to compare task completion times and scores. The calculations involved the following steps:

- Difference Calculation: Paired data for each subject before and after training were used to compute the differences.
- Averaging Differences: The average of all differences was calculated to assess the overall trend.
- Standard Error Calculation: The standard error was derived from the standard deviation of the differences to quantify variability.
- T-value and *p*-value Calculation: The t-value and *p*-value were computed based on the degrees of freedom (number of samples minus 1) to determine the significance of the differences.

The results of the paired-sample *t*-test included the t-value, degrees of freedom, and *p*-value. A *p*-value less than 0.05 indicated a statistically significant difference. In this study, the *t*-test results showed a significant reduction in task completion time after training, suggesting that the training effectively improved spatial cognitive abilities.

3.4. EEG Signal Acquisition and Pre-Processing

3.4.1. EEG Signal Acquisition

In this study, EEG signals were acquired using a 16-channel OpenBCI EEG amplifier with a sampling frequency of 1000 Hz during the spatial cognitive assessment tasks. Electrode caps were applied according to the international 10–20 system for electrode placement, and the EEG data were wirelessly transmitted to the computer's buffer via Wi-Fi.

3.4.2. EEG Signal Pre-Processing

During the spatial cognition assessment task, frequent hand and turning movements, along with artifacts such as ocular, electromyography (EMG), electrocardiography (ECG), and surrounding equipment noise, significantly affected the acquisition of EEG signals. To mitigate these effects, a series of preprocessing steps were applied to the raw EEG signals:

- Trap Filtering: The original EEG signals were band-pass filtered between 1–100 Hz using a Type I Chebyshev filter, followed by a 50 Hz notch filter to remove power-line interference.
- Fast Independent Component Analysis (ICA): ICA was applied to remove artifact interference from ocular, EMG, and ECG signals.
- Downsampling: The data sampling rate was reduced from 1000 Hz to 125 Hz using mean downsampling.
- Frequency Band Division: The EEG signals were band-pass filtered into seven frequency bands—Delta, Theta, Alpha1, Alpha2, Beta1, Beta2, and Gamma.
- Data Segmentation: EEG signals collected during the spatial localization and memory tasks were segmented using a moving window method with a window length of 4 s, a step size of 2 s, and a 50% overlap.

3.5. Experimental Sample Information

This experiment was approved by the Ethics Committee of the First Hospital of Qinhuangdao City, Hebei Province, China (Approval No. 2018B006). A total of 25 students from Yanshan University voluntarily participated in the study, including 19 males and 6 females, with an average age of 23.76 years (range: 21–28 years). Participants were divided into two groups based on the spatial cognitive training tasks they performed: a brain-controlled car group and a hand-controlled plane group.

The brain-controlled car group consisted of 13 participants (9 males and 4 females) with a mean age of 24.08 years (range: 21–28 years). The brain-controlled plane group included 12 participants (10 males and 2 females) with a mean age of 23.51 years (range: 21–25 years).

Inclusion criteria:

- Participants aged 18–30 years.
- Normal or corrected-to-normal vision and no significant hearing impairments.
- No history of neurological or psychiatric disorders, such as epilepsy or depression.
- No substance abuse or any condition that may affect cognitive function.
- Willing to participate in the experiment and provide informed consent.
- Exclusion criteria:
- Physical limitations that prevent prolonged use of VR equipment, such as neck pain.

- Consumption of medication that could affect cognitive abilities within 48 h prior to the experiment.
- Failure to comply with experimental protocols during training or testing phases.

Behavioral data and EEG signals were collected from all participants during the spatial cognition assessment tasks performed before and after the spatial cognition training.

4. Results

The assessment system proposed in this study integrates BCI, VR, and gesture recognition technologies to evaluate subjects' spatial cognitive abilities through cognitive assessment tasks. The experimental procedure consists of three stages: a baseline test conducted before training, continuous spatial cognition training, and a post-training ability test. During the testing phases, EEG signals and behavioral data were recorded simultaneously for subsequent feature extraction and cognitive ability evaluation.

4.1. Results of Behavioural Data

4.1.1. Evaluation of Task Completion Time

Figure 6 illustrates the task completion times of the brain-controlled car group during the spatial cognitive assessment task before and after training. The post-training task completion time was significantly reduced compared to the pre-training time. A paired-sample *t*-test revealed a highly significant difference between the two conditions, with the post-training time (191.23 $\pm$ 35.87 s) being significantly shorter than the pre-training time (264.38 $\pm$ 58.62 s), t(12) = 5.59, $p = 8.70 \times 10^{-5} < 0.01$.

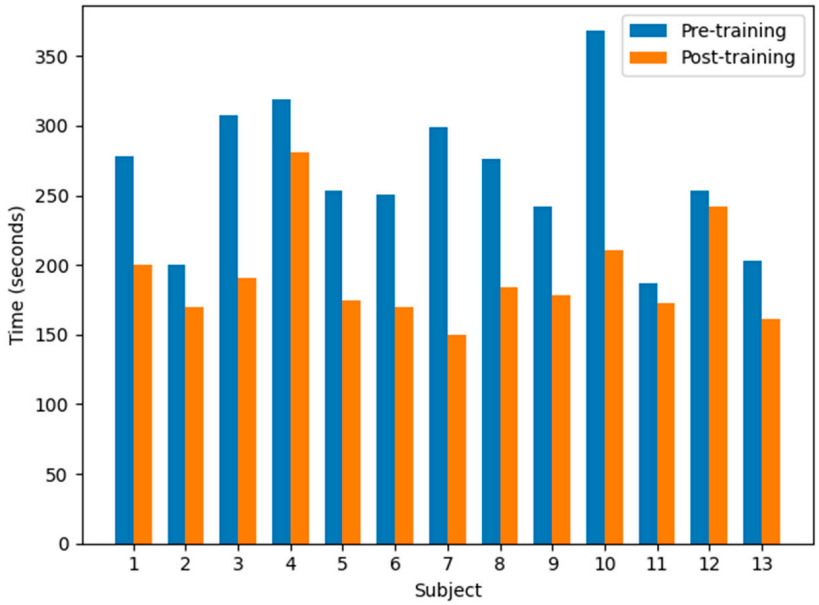

Figure 6. Bar chart of spatial cognitive assessment tasks time consumption for brain-controlled car group.

Figure 7 illustrates the task completion times of the brain-controlled plane group during the spatial cognitive assessment task before and after training. The post-training task completion time was significantly reduced compared to the pre-training time. A paired-sample *t*-test revealed a highly significant difference between the two conditions, with the post-training time (162.42 $\pm$ 35.04 s) being significantly shorter than the pre-training time (291.83 $\pm$ 92.07 s), t(11) = 6.02, $p = 0.00012 < 0.01$.

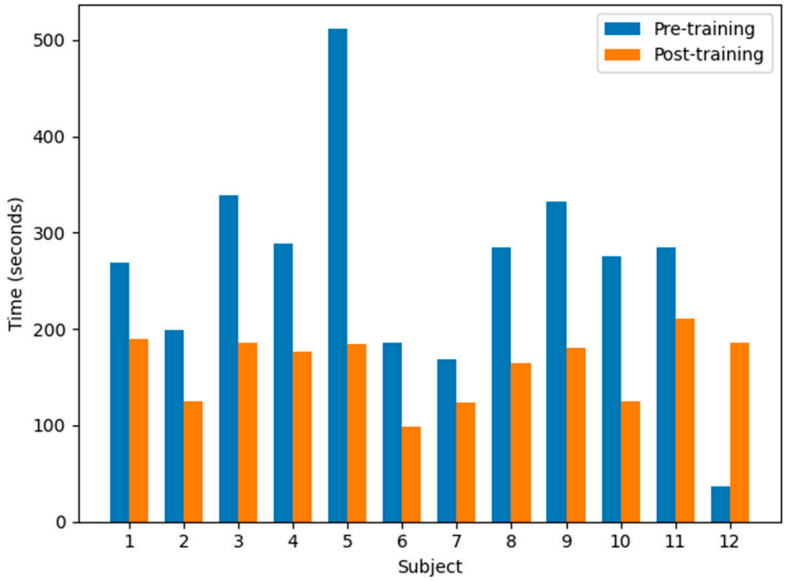

Figure 7. Bar chart of spatial cognitive assessment tasks time consumption for brain-controlled plane group.

4.1.2. Evaluation of Task Performance Scores

Figure 8 illustrates the scores of the brain-controlled car group in the spatial cognitive assessment task before and after training. Post-training scores showed a substantial increase compared to pre-training scores. A paired-sample *t*-test revealed a statistically significant difference, with post-training scores (15 ± 1.31) being significantly higher than pre-training scores (10 ± 2.93), $t(12) = -7.41$, $p = 8.15 \times 10^{-6} < 0.01$.

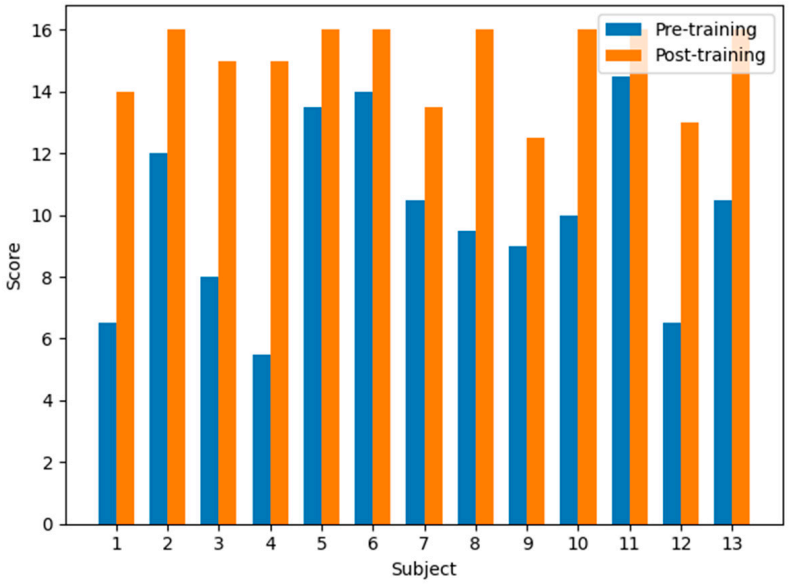

Figure 8. Bar chart of spatial cognitive assessment task scores for brain-controlled car group.

Figure 9 illustrates the ratings of the brain-controlled plane group on the spatial cognitive assessment task before and after training. Post-training scores showed a substantial increase compared to pre-training scores. A paired-sample *t*-test revealed a statistically significant difference, with post-training scores (15.13 ± 0.86) being significantly higher than pre-training scores (10.38 ± 2.71), $t(11) = -6.45$, $p = 4.50 \times 10^{-5} < 0.01$.

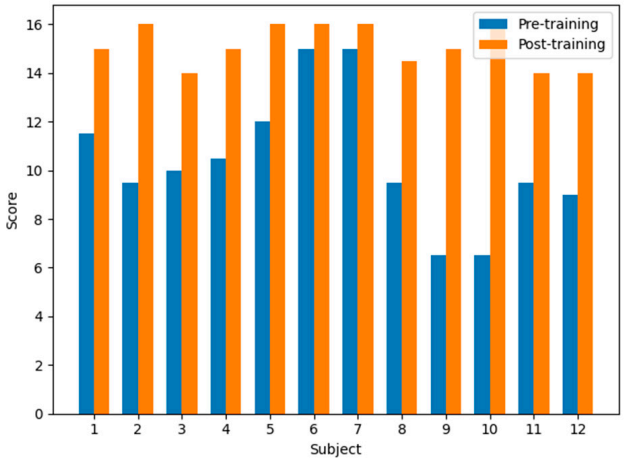

Figure 9. Bar chart of spatial cognitive assessment task scores for brain-controlled plane group.

4.2. EEG Signal Classification Performance

According to the SBS method, the optimal combinations of different EEG feature bands can be calculated as follows: Delta-Theta-Alpha1-Alpha2-Beta1-Beta2-Gamma, Delta-Alpha2-Beta1-Beta2-Gamma, Delta-Alpha2-Beta1-Beta2-Gamma, Delta-Alpha2-Beta2-Gamma, Delta-Alpha2-Gamma, and Delta-Gamma. Next, this paper will analyze the classification results for these 6 band combinations, respectively.

4.2.1. Dataset for Brain-Controlled Car Experiments

1. Delta-Theta-Alpha1-Alpha2-Beta1-Beta2-Gamma

Figures 10 and 11 illustrate the average validation accuracy and loss curves of EEG features based on PCMI, NPCMI, MPCMI, APCMI, and NAPCMI in CNN models.

In Figure 10, the average validation accuracy curves exhibit the following patterns:

- PCMI and NPCMI: Both stabilize after 180–200 iterations, with average validation accuracy between 96.5% and 96.6%.
- MPCMI: Stabilizes earlier, at 150–170 iterations, with an average validation accuracy of 97.2%.
- APCMI: Achieves a relatively high average validation accuracy of approximately 98.5%, stabilizing after 180–200 iterations.
- NAPCMI: Outperforms other methods, stabilizing at 100–120 iterations with an average validation accuracy of approximately 99.3%.

Figure 11 illustrates the average validation loss curves for PCMI, NPCMI, MPCMI, APCMI, and NAPCMI-based EEG features in CNN models. The results show the following patterns:

- PCMI and NPCMI: These models exhibit relatively high validation loss curves, with minimum loss values around 0.1.
- MPCMI: The validation loss curves are comparatively lower, with minimum loss values close to 0.07.
- APCMI: This model achieves a lower validation loss, with minimum loss values around 0.045.
- NAPCMI: Outperforms other methods with the lowest validation loss, having a minimum value close to 0.02.

Table 1 presents the average evaluation metrics of EEG features based on PCMI, NPCMI, MPCMI, APCMI, and NAPCMI in the CNN model. The results indicate the following:

- NAPCMI: Achieved the highest evaluation metrics, with a precision of 99.35%. Its corresponding F1 score, recall, and AUC values were significantly better than those of the other methods.
- APCMI and MPCMI: Showed relatively high performance, with precisions of 98.52% and 97.85%, respectively.
- NPCMI and PCMI: Displayed lower evaluation results, with accuracies around 96.6%.

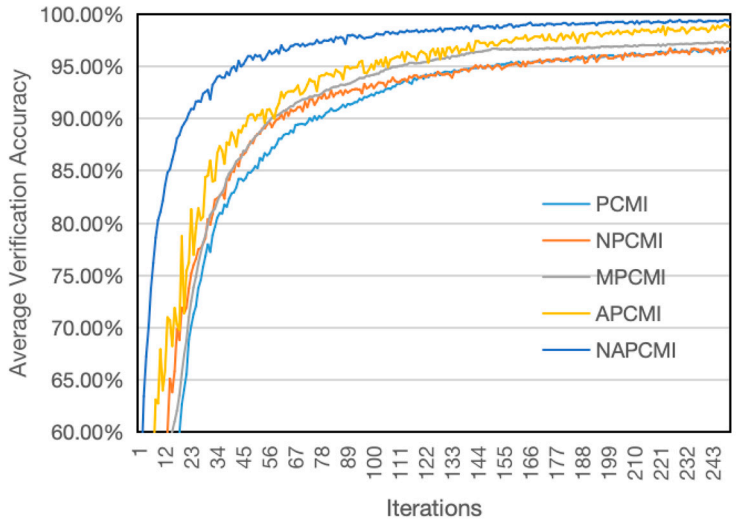

Figure 10. Average accuracy curve of Delta-Theta-Alpha1-Alpha2-Beta1-Beta2-Gamma frequency band combination for brain-controlled car group.

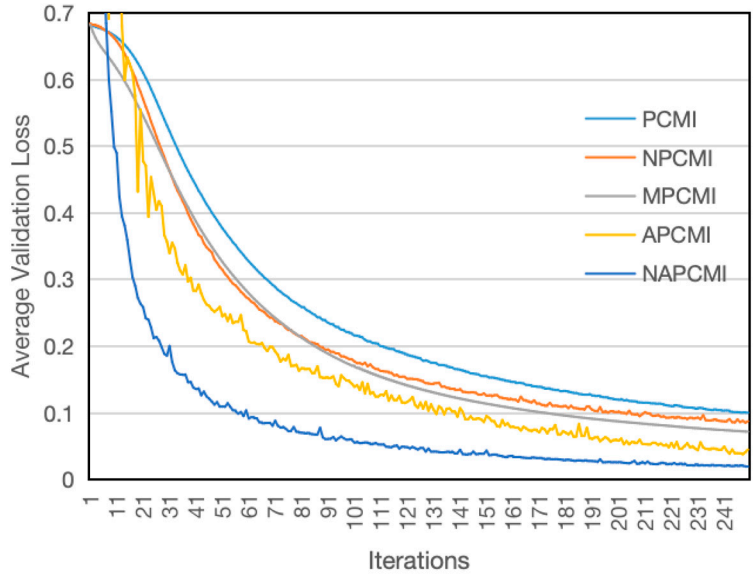

Figure 11. Average loss curve of Delta-Theta-Alpha1-Alpha2-Beta1-Beta2-Gamma band combination for brain-controlled car group.

Table 1. Average evaluation index of Delta-Theta-Alpha1-Alpha2-Beta1-Beta2-Gamma for brain-controlled car group.

Feature Extraction Methods	Precision	Recall	F1-Score	AUC
PCMI	96.57%	96.57%	96.57%	0.990
NPCMI	96.68%	96.68%	96.68%	0.991
MPCMI	97.85%	97.85%	97.85%	0.993
APCMI	98.52%	98.52%	98.52%	0.994
NAPCMI	99.35%	99.35%	99.35%	0.995

2. Delta-Theta-Alpha2-Beta1-Beta2-Gamma

Figures 12 and 13 illustrate the average validation accuracy and loss curves of EEG features based on PCMI, NPCMI, MPCMI, APCMI, and NAPCMI in the CNN model.

- PCMI and NPCMI: The validation accuracy curves are similar, stabilizing at 180–200 iterations, with average validation accuracies of approximately 95.8% and 96.5%, respectively.
- MPCMI and APCMI: These methods achieve higher validation accuracies, stabilizing at 170–180 iterations, with average accuracies of 97.2% and 97.8%, respectively.
- NAPCMI: Exhibits the highest performance, stabilizing at 140–160 iterations, with an average validation accuracy of approximately 98.5%.

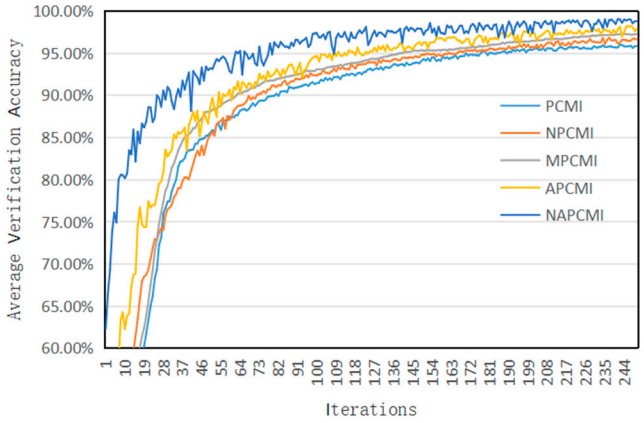

Figure 12. Average accuracy curve of Delta-Theta-Alpha2-Beta1-Beta2-Gamma frequency band combination for brain-controlled car group.

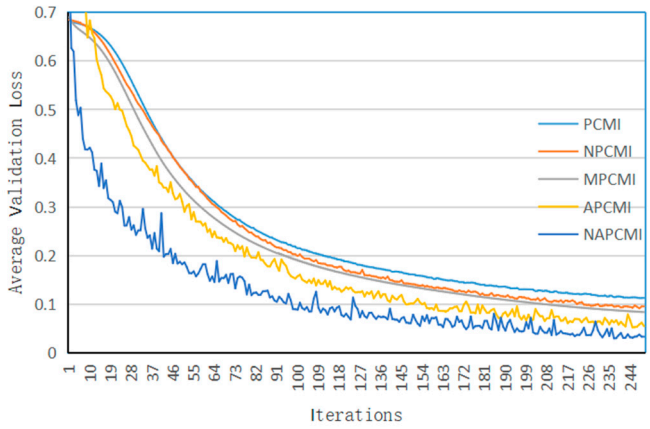

Figure 13. Average loss curve of Delta-Theta-Alpha2-Beta1-Beta2-Gamma band combination for brain-controlled car group.

The average validation loss profiles for PCMI and NPCMI EEG features are relatively high, with minimum values around 0.1. In contrast, MPCMI and APCMI EEG features exhibit lower validation loss profiles, with minimum values of approximately 0.06 and 0.05, respectively. NAPCMI EEG features achieve the lowest validation loss, with a minimum value close to 0.035.

Table 2 presents the average evaluation metrics of EEG features based on PCMI, NPCMI, MPCMI, APCMI, and NAPCMI in CNN models. NAPCMI-based EEG features achieved the highest accuracy (98.77%), significantly outperforming the other methods. MPCMI- and APCMI-based EEG features also performed well, with accuracies of 97.15% and 97.90%, respectively. In contrast, NPCMI- and PCMI-based EEG features showed lower accuracies of 96.81% and 95.92%, respectively.

Table 2. Average evaluation index of Delta-Theta-Alpha2-Beta1-Beta2-Gamma for brain-controlled car group.

Feature Extraction Methods	Precision	Recall	F1-Score	AUC
PCMI	95.92%	95.92%	95.92%	0.989
NPCMI	96.81%	96.81%	96.81%	0.991
MPCMI	97.16%	97.16%	97.16%	0.991
APCMI	97.90%	97.90%	97.90%	0.994
NAPCMI	98.77%	98.77%	98.77%	0.995

3. Delta-Alpha2-Beta1-Beta2-Gamma

Figures 14 and 15 illustrate the average validation accuracy and loss curves of EEG features based on PCMI, NPCMI, MPCMI, APCMI, and NAPCMI in the CNN model.

- PCMI and NPCMI: The validation accuracy curves are similar, stabilizing at 180–200 iterations with average validation accuracies of approximately 95.3%.
- MPCMI and APCMI: These methods achieve higher validation accuracies, stabilizing at 160–180 iterations, with average accuracies of 96.3% and 98.3%, respectively.
- NAPCMI: Exhibits the highest validation accuracy, stabilizing at 140–160 iterations with an average accuracy of approximately 98.6%.

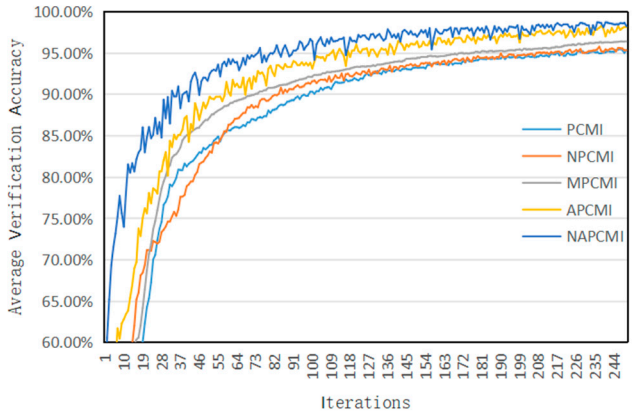

Figure 14. Average accuracy curve of Delta-Alpha2-Beta1-Beta2-Gamma frequency band combination for brain-controlled car group.

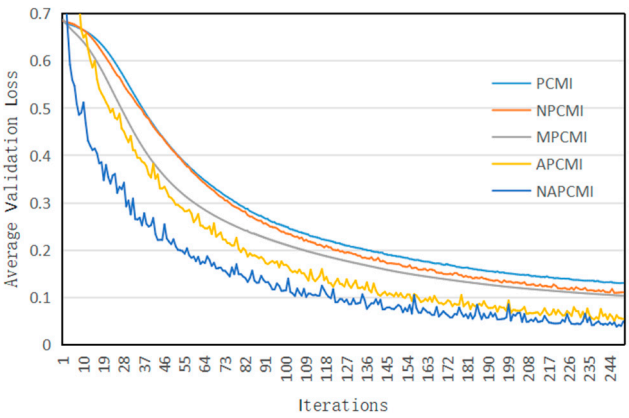

Figure 15. Average loss curve of Delta-Alpha2-Beta1-Beta2-Gamma band combination for brain-controlled car group.

Figure 15 illustrates the average validation loss curves for EEG features based on PCMI, NPCMI, MPCMI, APCMI, and NAPCMI in CNN models. The validation loss curves for PCMI, NPCMI, and MPCMI EEG features are relatively high, with minimum loss

values around 0.12. In contrast, APCMI EEG features exhibit lower validation loss, with a minimum value close to 0.05. NAPCMI EEG features achieve the lowest validation loss, with a minimum value close to 0.04.

Table 3 presents the average evaluation metrics of EEG features based on PCMI, NPCMI, MPCMI, APCMI, and NAPCMI in the CNN model. NAPCMI-based EEG features achieved the highest precision (98.21%) and demonstrated superior F1 scores, recall rates, AUC values, and other metrics compared to the other methods. APCMI-based EEG features also performed well, with a precision of 98.02%. In contrast, EEG features based on MPCMI, NPCMI, and PCMI yielded relatively lower results, with accuracies around 95.5%.

Table 3. Average evaluation index of Delta-Alpha2-Beta1-Beta2-Gamma for brain-controlled car group.

Feature Extraction Methods	Precision	Recall	F1-Score	AUC
PCMI	95.46%	95.46%	95.46%	0.985
NPCMI	95.45%	95.45%	95.45%	0.989
MPCMI	96.45%	96.45%	96.45%	0.990
APCMI	98.02%	98.02%	98.02%	0.994
NAPCMI	98.21%	98.21%	98.21%	0.994

4. Delta-Alpha2-Beta2-Gamma

Figures 16 and 17 illustrate the average validation accuracy and loss curves of EEG features based on PCMI, NPCMI, MPCMI, APCMI, and NAPCMI in CNN models.

- PCMI and NPCMI: The validation accuracy curves are similar, stabilizing at 200–220 iterations with average accuracies of approximately 93.3% and 92.8%, respectively.
- MPCMI and APCMI: These methods achieve higher accuracies, stabilizing at 180–200 iterations with average accuracies of 95.9% and 96.8%, respectively.
- NAPCMI: Exhibits the highest validation accuracy, stabilizing at 140–160 iterations with an average accuracy of approximately 98.8%.

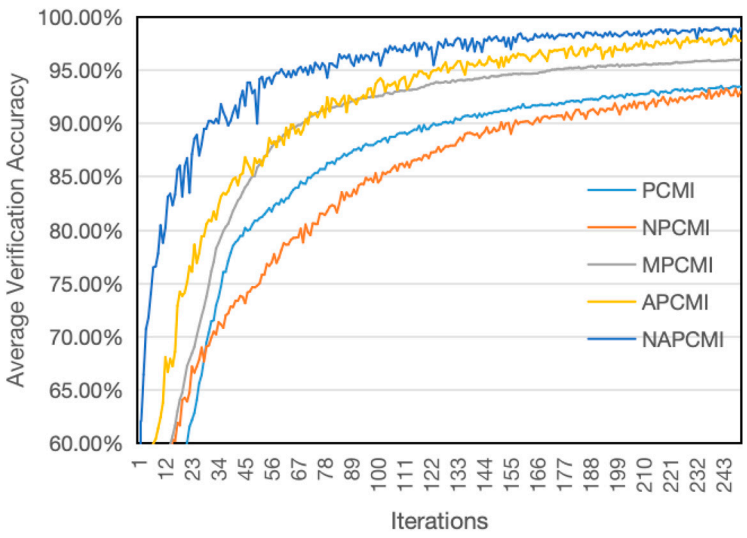

Figure 16. Average accuracy curve of Delta-Alpha2-Beta2-Gamma frequency band combination for brain-controlled car group.

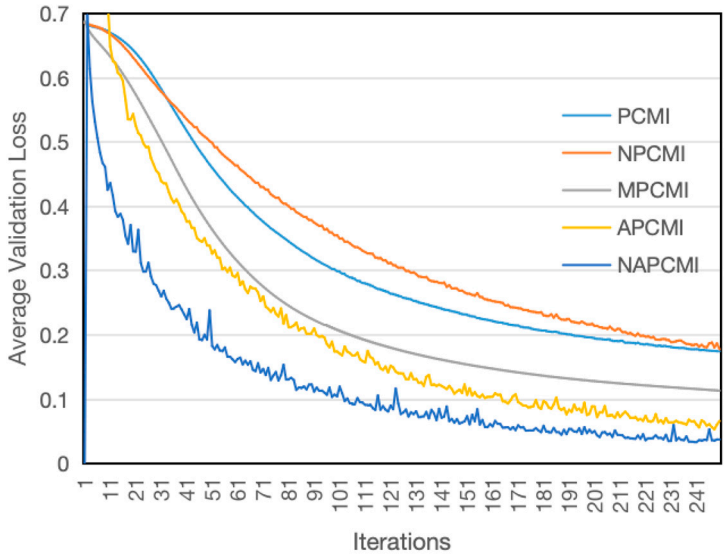

Figure 17. Average loss curve of Delta-Alpha2-Beta2-Gamma band combination for brain-controlled car group.

Figure 17 illustrates the average validation loss curves for EEG features based on PCMI, NPCMI, MPCMI, APCMI, and NAPCMI in CNN models.

- PCMI and NPCMI: The validation loss curves are relatively high, with minimum loss values around 0.17.
- MPCMI and APCMI: These methods exhibit lower validation loss curves, with minimum values of approximately 0.011 and 0.065, respectively.
- NAPCMI: Achieves the lowest validation loss, with minimum values close to 0.035.

Table 4 presents the average evaluation metrics of EEG features based on PCMI, NPCMI, MPCMI, APCMI, and NAPCMI in the CNN model. NAPCMI-based EEG features achieved the highest accuracy (98.93%), significantly outperforming the other methods. MPCMI- and APCMI-based features showed relatively high accuracies of approximately 96% and 97.7%, respectively. In contrast, NPCMI- and PCMI-based features yielded lower accuracies, both around 93%.

Table 4. Average evaluation index of Delta-Alpha2-Beta2-Gamma for brain-controlled car group.

Feature Extraction Methods	Precision	Recall	F1-Score	AUC
PCMI	93.47%	93.47%	93.47%	0.978
NPCMI	93.04%	93.04%	93.04%	0.978
MPCMI	96.00%	96.00%	96.00%	0.987
APCMI	97.78%	97.78%	97.78%	0.994
NAPCMI	98.93%	98.93%	98.93%	0.995

5. Delta-Alpha2-Gamma

Figures 18 and 19 illustrate the average validation accuracy and loss curves of EEG features based on PCMI, NPCMI, MPCMI, APCMI, and NAPCMI in the CNN model.

- PCMI and NPCMI: The validation accuracy curves are similar, stabilizing at 180–200 iterations with average accuracies of approximately 92.1%.
- MPCMI and APCMI: These methods achieve higher validation accuracies, stabilizing at 160–180 iterations with average accuracies of 94.8% and 97.3%, respectively.
- NAPCMI: Outperforms the other methods, stabilizing at 140–160 iterations with the highest average validation accuracy of approximately 98.4%.

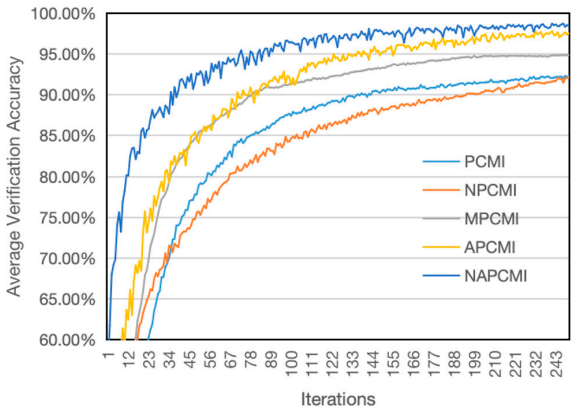

Figure 18. Average accuracy curve of Delta-Alpha2-Gamma frequency band combination for brain-controlled car group.

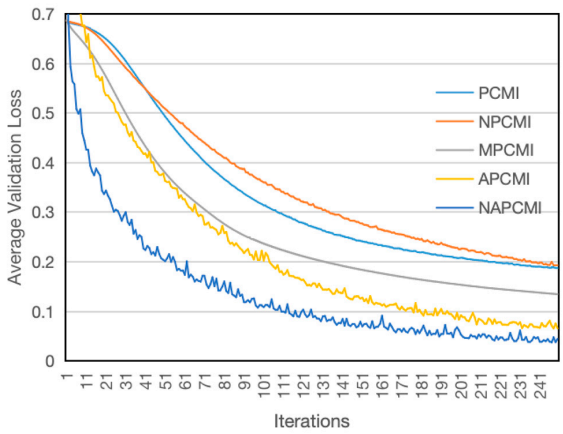

Figure 19. Average loss curve of Delta-Alpha2-Gamma band combination for brain-controlled car group.

Figure 19 illustrates the average validation loss curves for EEG features based on PCMI, NPCMI, MPCMI, APCMI, and NAPCMI in CNN models.

- PCMI and NPCMI: These methods exhibit relatively high validation loss curves, with minimum loss values around 0.186.
- MPCMI and APCMI: The validation loss curves are lower, with minimum values of approximately 0.134 and 0.065, respectively.
- NAPCMI: Achieves the lowest validation loss, with minimum values close to 0.044.

Table 5 presents the average evaluation metrics of EEG features based on PCMI, NPCMI, MPCMI, APCMI, and NAPCMI in the CNN model. NAPCMI-based EEG features achieved the highest accuracy (98.41%), significantly outperforming the other methods. MPCMI- and APCMI-based features showed relatively high accuracies of 94.95% and 97.49%, respectively. In contrast, NPCMI- and PCMI-based features yielded lower accuracies, both around 92%.

Table 5. Average evaluation index of Delta-Alpha2-Gamma for brain-controlled car group.

Feature Extraction Methods	Precision	Recall	F1-Score	AUC
PCMI	92.23%	92.23%	92.23%	0.974
NPCMI	92.28%	92.28%	92.28%	0.976
MPCMI	94.95%	94.95%	94.95%	0.985
APCMI	97.49%	97.49%	97.49%	0.993
NAPCMI	98.41%	98.41%	98.41%	0.994

6. Delta-Gamma

Figures 20 and 21 illustrate the average validation accuracy and loss curves of EEG features based on PCMI, NPCMI, MPCMI, APCMI, and NAPCMI in the CNN model.

- PCMI and NPCMI: The validation accuracy curves are similar, stabilizing at 200–220 iterations with average accuracies around 90%.
- MPCMI and APCMI: These methods achieve higher accuracies, stabilizing at 180–200 iterations with average accuracies of 94.3% and 97.0%, respectively.
- NAPCMI: Outperforms other methods, stabilizing at 140–160 iterations with the highest average validation accuracy of approximately 98.6%.

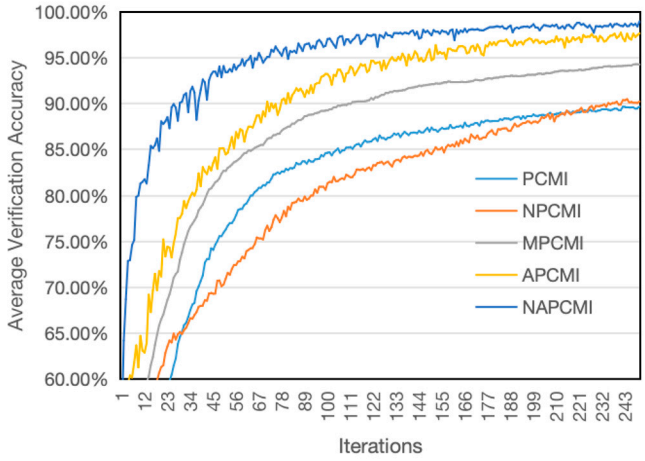

Figure 20. Average accuracy curve of Delta-Gamma frequency band combination for brain-controlled car group.

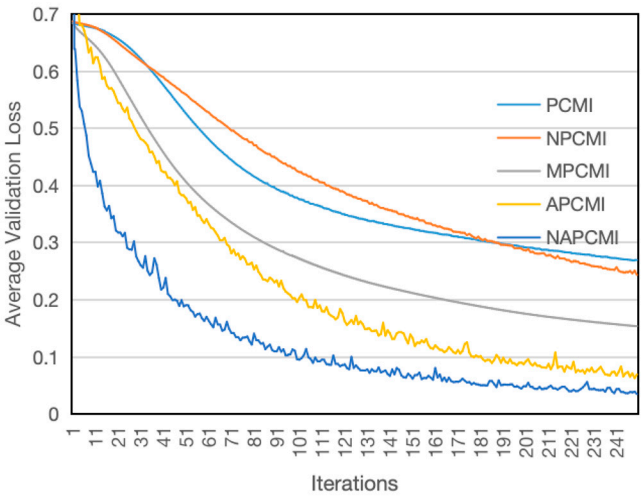

Figure 21. Average loss curve of Delta-Gamma band combination for brain-controlled car group.

Figure 21 illustrates the average validation loss curves for EEG features based on PCMI, NPCMI, MPCMI, APCMI, and NAPCMI in CNN models.

- PCMI and NPCMI: The validation loss curves are relatively high, with minimum values around 0.256.
- MPCMI and APCMI: These methods exhibit lower validation losses, with minimum values of approximately 0.154 and 0.065, respectively.
- NAPCMI: Achieves the lowest validation loss, with a minimum value close to 0.034.

Table 6 presents the average evaluation metrics of EEG features based on PCMI, NPCMI, MPCMI, APCMI, and NAPCMI in CNN models. NAPCMI-based EEG features

achieved the highest accuracy (98.91%), significantly outperforming the other methods. MPCMI- and APCMI-based features demonstrated relatively high accuracies of 94.39% and 97.62%, respectively. In contrast, NPCMI- and PCMI-based features yielded lower accuracies, both around 90%.

Table 6. Average evaluation index of Delta-Gamma for brain-controlled car group.

Feature Extraction Methods	Precision	Recall	F1-Score	AUC
PCMI	89.77%	89.77%	89.77%	0.952
NPCMI	90.30%	90.30%	90.30%	0.952
MPCMI	94.39%	94.39%	94.39%	0.981
APCMI	97.62%	97.62%	97.62%	0.993
NAPCMI	98.91%	98.91%	98.91%	0.994

4.2.2. Dataset for Hand-Controlled Plane Experiments

1. Delta-Theta-Alpha1-Alpha2-Beta1-Beta2-Gamma

Figures 22 and 23 illustrate the average validation accuracy and loss curves of EEG features based on PCMI, NPCMI, MPCMI, APCMI, and NAPCMI in CNN models.

- PCMI and NPCMI: The validation accuracy curves are similar, stabilizing at 180–200 iterations with average accuracies of around 96.6%.
- MPCMI and APCMI: These methods achieve higher accuracies, stabilizing at 160–180 iterations with average accuracies of 97.7% and 98.0%, respectively.
- NAPCMI: Exhibits the highest accuracy, stabilizing at 140–160 iterations with an average validation accuracy of approximately 99.5%.

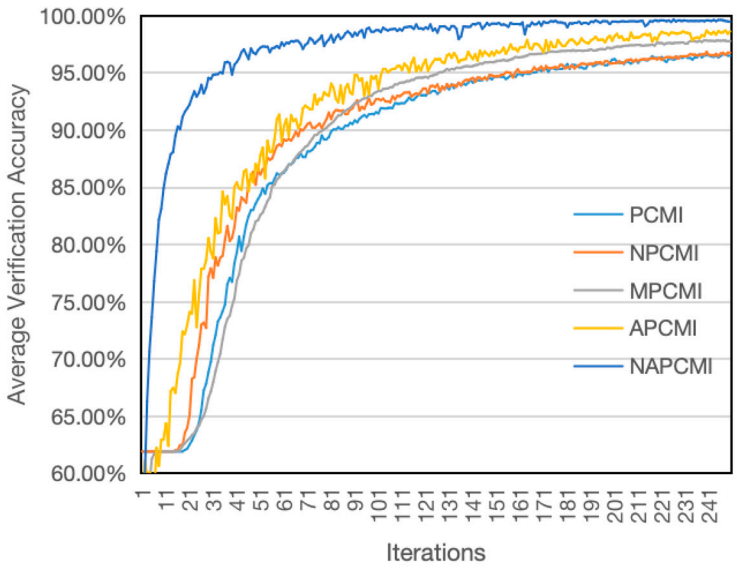

Figure 22. Average accuracy curve of Delta-Theta-Alpha1-Alpha2-Beta1-Beta2-Gamma frequency band combination for brain-controlled plane group.

Figure 23 illustrates the average validation loss curves for EEG features based on PCMI, NPCMI, MPCMI, APCMI, and NAPCMI in CNN models.

- PCMI and NPCMI: The validation loss curves are relatively high, with minimum values around 0.1.
- MPCMI and APCMI: These methods exhibit lower validation loss curves, with minimum values of approximately 0.065 and 0.052, respectively.
- NAPCMI: Achieves the lowest validation loss, with a minimum value close to 0.013.

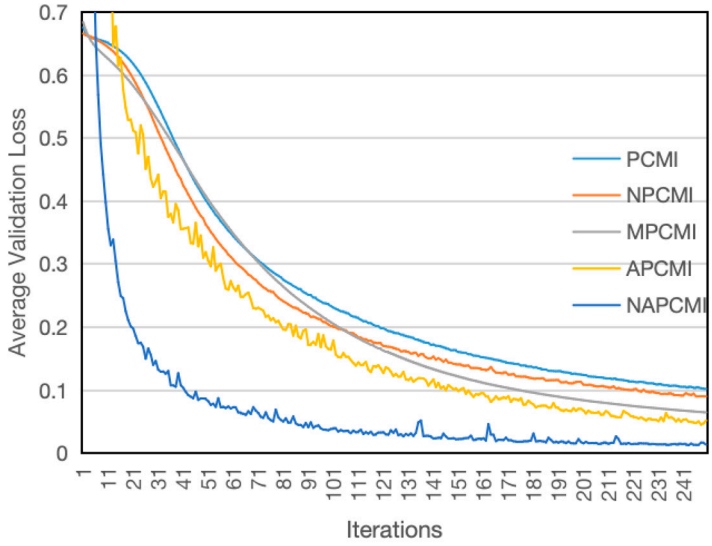

Figure 23. Average loss curve of Delta-Theta-Alpha1-Alpha2-Beta1-Beta2-Gamma band combination for brain-controlled plane group.

Table 7 presents the average evaluation metrics of EEG features based on PCMI, NPCMI, MPCMI, APCMI, and NAPCMI in the CNN model. NAPCMI-based EEG features achieved the highest accuracy (99.50%), significantly outperforming the other methods. MPCMI- and APCMI-based features also demonstrated high accuracies, both around 98%. In contrast, NPCMI- and PCMI-based features yielded lower accuracies, approximately 96%.

Table 7. Average evaluation index of Delta-Theta-Alpha1-Alpha2-Beta1-Beta2-Gamma for brain-controlled plane group.

Feature Extraction Methods	Precision	Recall	F1-Score	AUC
PCMI	89.77%	89.77%	89.77%	0.952
NPCMI	90.30%	90.30%	90.30%	0.952
MPCMI	94.39%	94.39%	94.39%	0.981
APCMI	97.62%	97.62%	97.62%	0.993
NAPCMI	98.91%	98.91%	98.91%	0.994

2. Delta-Theta-Alpha2-Beta1-Beta2-Gamma

Figures 24 and 25 illustrate the average validation accuracy and loss curves for EEG features based on PCMI, NPCMI, MPCMI, APCMI, and NAPCMI in CNN models.

- PCMI, NPCMI, and MPCMI: These methods exhibit similar validation accuracy curves, stabilizing at 180–200 iterations with accuracies around 96%.
- APCMI: The validation accuracy curve is relatively higher, stabilizing at 180–200 iterations with an accuracy of 97.5%.
- NAPCMI: Outperforms all other methods, stabilizing at 140–160 iterations with the highest validation accuracy of approximately 98.1%.

Figure 25 illustrates the average validation loss curves for EEG features based on PCMI, NPCMI, MPCMI, APCMI, and NAPCMI in CNN models.

- PCMI, NPCMI, and MPCMI: These methods exhibit the highest validation loss curves, with minimum values around 0.1.
- APCMI: The validation loss is relatively low, with a minimum value close to 0.07.
- NAPCMI: Achieves the lowest validation loss, with a minimum value close to 0.045.

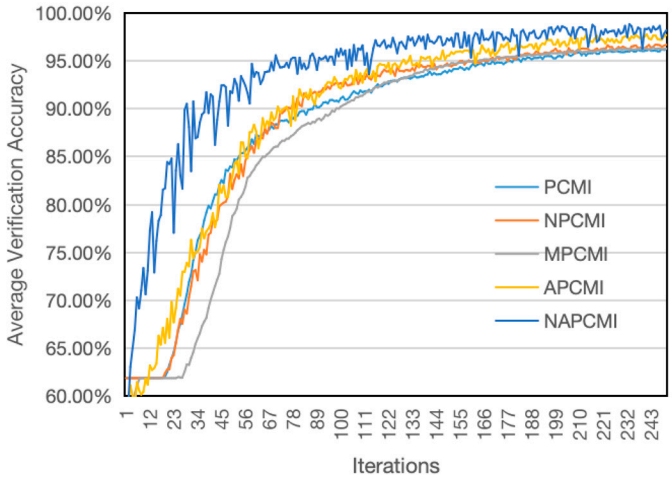

Figure 24. Average accuracy curve of Delta-Theta-Alpha2-Beta1-Beta2-Gamma frequency band combination for brain-controlled plane group.

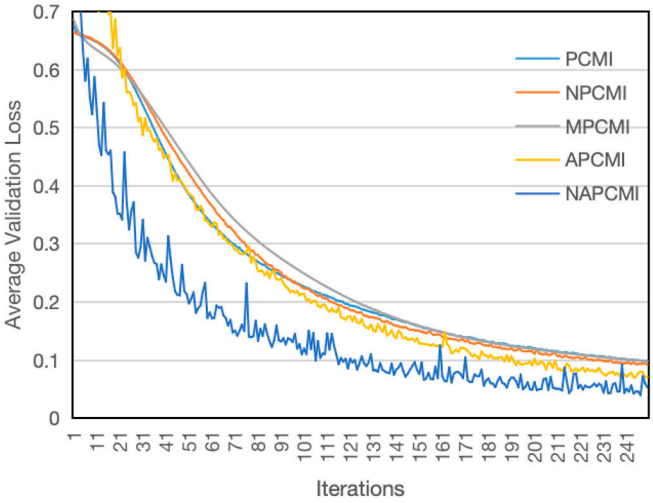

Figure 25. Average loss curve of Delta-Theta-Alpha2-Beta1-Beta2-Gamma band combination for brain-controlled plane group.

Table 8 presents the average evaluation metrics of EEG features based on PCMI, NPCMI, MPCMI, APCMI, and NAPCMI in the CNN model. NAPCMI-based features achieved the highest accuracy (98.17%), significantly outperforming the other methods. APCMI-based features also demonstrated high performance, with an accuracy of 97.53%. In contrast, features based on MPCMI, NPCMI, and PCMI yielded lower accuracies, around 96%.

Table 8. Average evaluation index of Delta-Theta-Alpha2-Beta1-Beta2-Gamma for brain-controlled plane group.

Feature Extraction Methods	Precision	Recall	F1-Score	AUC
PCMI	96.08%	96.08%	96.08%	0.990
NPCMI	96.58%	96.58%	96.58%	0.990
MPCMI	96.35%	96.35%	96.35%	0.990
APCMI	97.53%	97.53%	97.53%	0.994
NAPCMI	98.17%	98.17%	98.17%	0.994

3. Delta-Alpha2-Beta1-Beta2-Gamma

Figures 26 and 27 illustrate the average validation accuracy and loss curves for EEG features based on PCMI, NPCMI, MPCMI, APCMI, and NAPCMI in CNN models.

- PCMI, NPCMI, MPCMI, and APCMI: These methods exhibit similar validation accuracy curves, stabilizing at 180–200 iterations with accuracies around 96%.
- NAPCMI: Achieves the highest validation accuracy, stabilizing at 140–160 iterations with an accuracy of 98.7%.

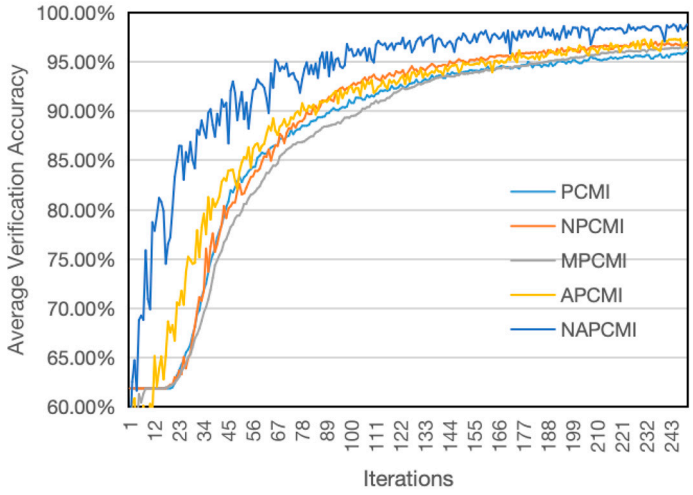

Figure 26. Average accuracy curve of Delta-Alpha2-Beta1-Beta2-Gamma frequency band combination for brain-controlled plane group.

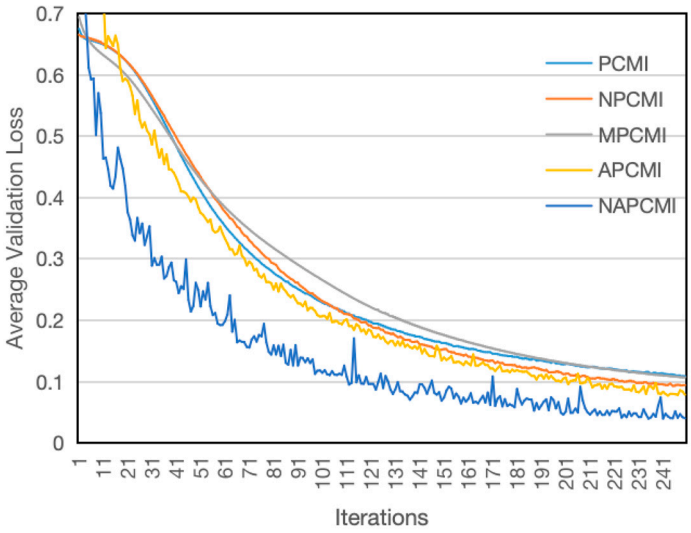

Figure 27. Average loss curve of Delta-Alpha2-Beta1-Beta2-Gamma band combination for brain-controlled plane group.

Figure 27 illustrates the average validation loss curves for EEG features based on PCMI, NPCMI, MPCMI, APCMI, and NAPCMI in CNN models.

- PCMI, NPCMI, and MPCMI: These methods exhibit high validation loss curves, with minimum values around 0.1.
- APCMI: The validation loss is relatively lower, with a minimum value close to 0.08.
- NAPCMI: Achieves the lowest validation loss, with a minimum value close to 0.04.

Table 9 presents the average evaluation metrics of EEG features based on PCMI, NPCMI, MPCMI, APCMI, and NAPCMI in the CNN model. NAPCMI-based features

achieved the highest accuracy (98.79%), significantly outperforming the other methods. APCMI-based features also performed well, with an accuracy of 96.87%. In contrast, features based on MPCMI, NPCMI, and PCMI yielded lower accuracies, around 96%.

Table 9. Average evaluation index of Delta-Alpha2-Beta1-Beta2-Gamma for brain-controlled plane group.

Feature Extraction Methods	Precision	Recall	F1-Score	AUC
PCMI	95.99%	95.99%	95.99%	0.989
NPCMI	96.44%	96.44%	96.44%	0.991
MPCMI	96.42%	96.42%	96.42%	0.990
APCMI	96.87%	96.87%	96.87%	0.992
NAPCMI	98.79%	98.79%	98.79%	0.995

4. Delta-Alpha2-Beta2-Gamma

Figures 28 and 29 illustrate the average validation accuracy and loss curves for EEG features based on PCMI, NPCMI, MPCMI, APCMI, and NAPCMI in CNN models.

- PCMI: Exhibits the lowest validation accuracy, stabilizing at 200–220 iterations with an accuracy of approximately 93.8%.
- NPCMI and MPCMI: These methods achieve relatively low validation accuracies, stabilizing at 180–200 iterations with accuracies around 95%.
- APCMI: Demonstrates higher validation accuracy, stabilizing at 180–200 iterations with an accuracy of approximately 96.8%.
- NAPCMI: Achieves the highest validation accuracy, stabilizing at 140–160 iterations with an accuracy of approximately 97.8%.

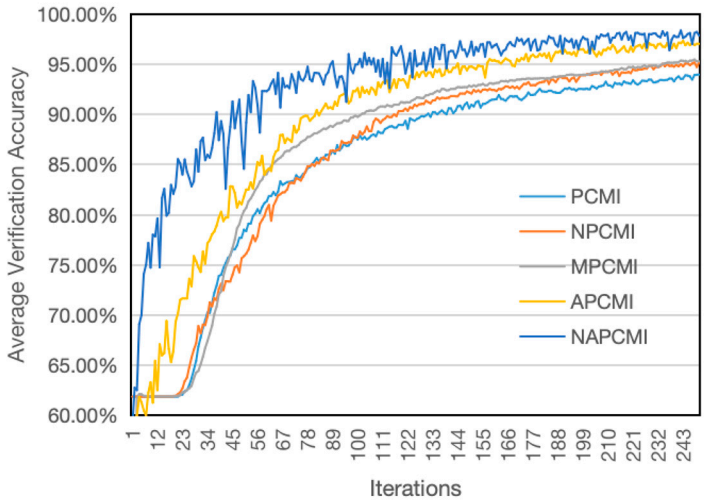

Figure 28. Average accuracy curve of Delta-Alpha2-Beta2-Gamma frequency band combination for brain-controlled plane group.

Figure 29 illustrates the average validation loss curves for EEG features based on PCMI, NPCMI, MPCMI, APCMI, and NAPCMI in CNN models.

- PCMI: Exhibits a relatively high validation loss, with a minimum value of around 0.15.
- NPCMI and MPCMI: Both demonstrate moderately high validation losses, with minimum values around 0.126.
- APCMI and NAPCMI: Achieve relatively low validation losses, with minimum values close to 0.08.

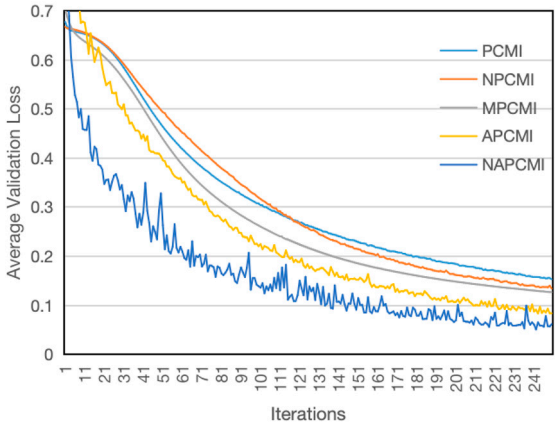

Figure 29. Average loss curve of Delta-Alpha2-Beta2-Gamma band combination for brain-controlled plane group.

Table 10 presents the average evaluation metrics of EEG features based on PCMI, NPCMI, MPCMI, APCMI, and NAPCMI in the CNN model. NAPCMI-based features achieved the highest accuracy (97.82%), significantly outperforming the other methods. APCMI-based features also performed well, with an accuracy of approximately 96.8%. In contrast, MPCMI-, NPCMI-, and PCMI-based features yielded lower accuracies of 95% and 93%, respectively.

Table 10. Average evaluation index of Delta-Alpha2-Beta2-Gamma for brain-controlled plane group.

Feature Extraction Methods	Precision	Recall	F1-Score	AUC
PCMI	93.80%	93.80%	93.80%	0.983
NPCMI	94.97%	94.97%	94.97%	0.985
MPCMI	95.42%	96.42%	95.42%	0.987
APCMI	96.81%	96.81%	96.81%	0.993
NAPCMI	97.82%	97.82%	97.82%	0.994

5. Delta-Alpha2-Gamma

Figures 30 and 31 illustrate the average validation accuracy and loss curves for EEG features based on PCMI, NPCMI, MPCMI, APCMI, and NAPCMI in CNN models.

- PCMI, NPCMI, and MPCMI: These methods exhibit similar validation accuracy curves, stabilizing at 200–220 iterations with average accuracies of around 93.2%.
- APCMI: Demonstrates higher validation accuracy, stabilizing at 180–200 iterations with average accuracies of approximately 95.7%.
- NAPCMI: Achieves the highest validation accuracy, stabilizing at 160–180 iterations with an accuracy of about 98.7%.

Figure 31 illustrates the average validation loss curves for EEG features based on PCMI, NPCMI, MPCMI, APCMI, and NAPCMI in CNN models.

- PCMI, NPCMI, and MPCMI: These methods exhibit relatively high validation loss curves, with minimum values around 0.16.
- APCMI: Demonstrates lower validation losses, with a minimum value close to 0.08.
- NAPCMI: Achieves the lowest validation loss, with a minimum value close to 0.05.

Table 11 presents the average evaluation metrics of EEG features based on PCMI, NPCMI, MPCMI, APCMI, and NAPCMI in the CNN model. NAPCMI-based features achieved the highest accuracy (98.72%), significantly outperforming the other methods. APCMI-based features also demonstrated strong performance, with an accuracy

of 96.53%. In contrast, MPCMI-, NPCMI-, and PCMI-based features yielded lower accuracies, around 93%.

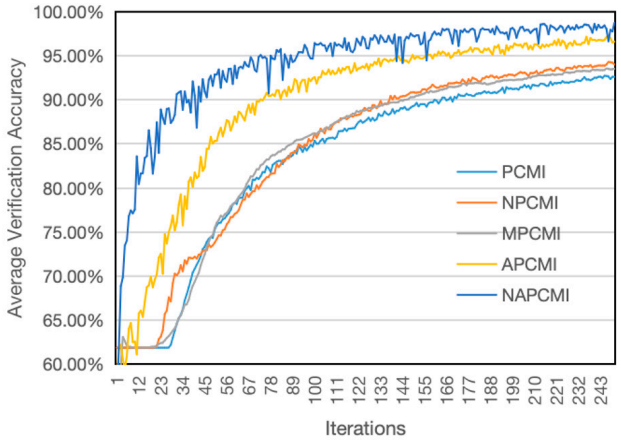

Figure 30. Average accuracy curve of Delta-Alpha2-Gamma frequency band combination for brain-controlled plane group.

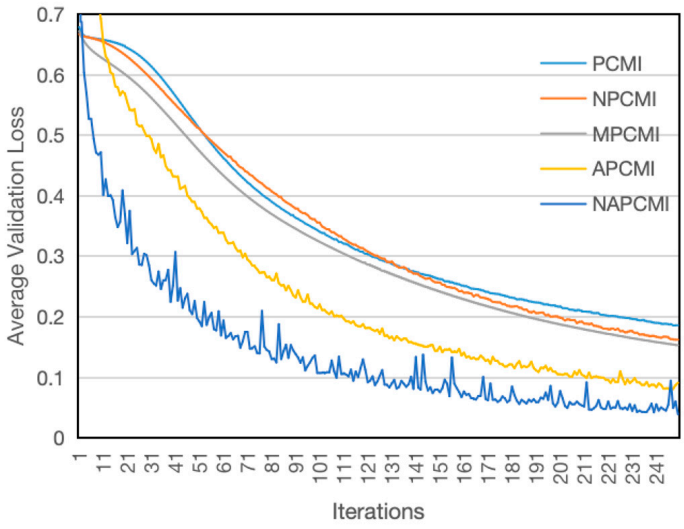

Figure 31. Average loss curve of Delta-Alpha2-Gamma band combination for brain-controlled plane group.

Table 11. Average evaluation index of Delta-Alpha2-Gamma for brain-controlled plane group.

Feature Extraction Methods	Precision	Recall	F1-Score	AUC
PCMI	92.32%	92.32%	92.32%	0.974
NPCMI	93.49%	93.49%	93.49%	0.982
MPCMI	93.62%	93.62%	93.62%	0.982
APCMI	96.53%	96.53%	96.53%	0.992
NAPCMI	98.72%	98.72%	98.72%	0.995

6. Delta-Gamma

Figures 32 and 33 illustrate the average validation accuracy and loss curves for EEG features based on PCMI, NPCMI, MPCMI, APCMI, and NAPCMI in CNN models.

- PCMI: Exhibits the lowest validation accuracy, stabilizing at 200–220 iterations with an accuracy of approximately 91%.
- NPCMI and MPCMI: These methods demonstrate moderate validation accuracies, stabilizing at 200–220 iterations with accuracies around 93%.

- APCMI: Achieves relatively high validation accuracy, stabilizing at 180–200 iterations with an accuracy of approximately 96%.
- NAPCMI: Outperforms all other methods, stabilizing at 160–180 iterations with the highest accuracy of about 97%.

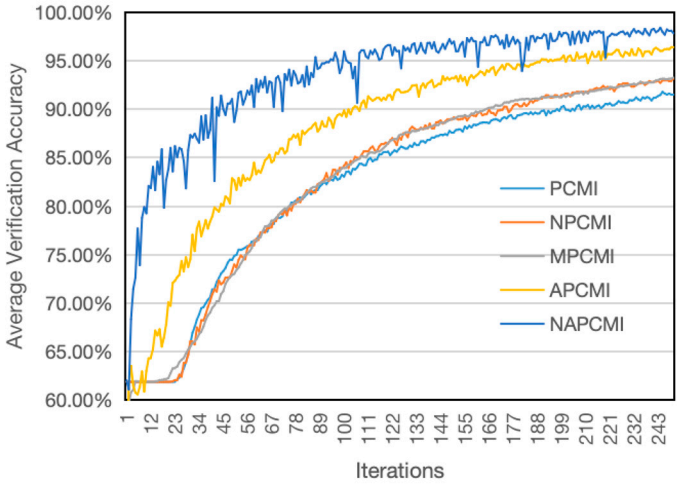

Figure 32. Average accuracy curve of Delta-Gamma frequency band combination for brain-controlled plane group.

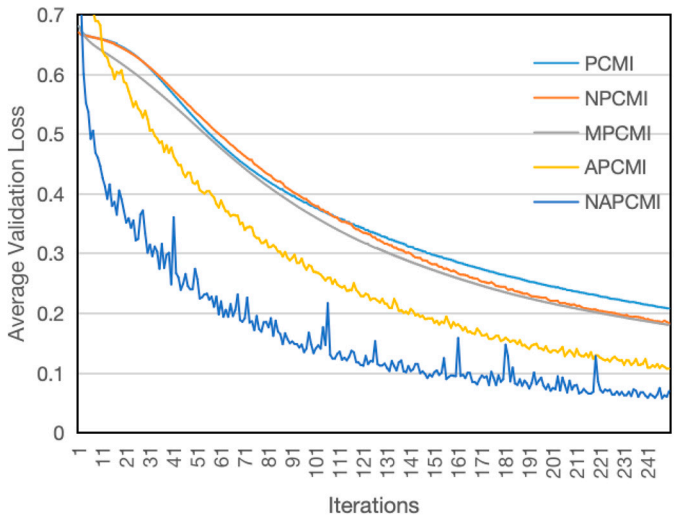

Figure 33. Average loss curve of Delta-Gamma band combination for brain-controlled plane group.

Figure 33 illustrates the average validation loss curves for EEG features based on PCMI, NPCMI, MPCMI, APCMI, and NAPCMI in CNN models.

- PCMI: Exhibits relatively high validation loss, with a minimum value of around 0.2.
- NPCMI, MPCMI, and APCMI: These methods demonstrate lower validation losses, with minimum values around 0.18 and 0.1, respectively.
- NAPCMI: Achieves the lowest validation loss, with a minimum value close to 0.06.

Table 12 presents the average evaluation metrics of EEG features based on PCMI, NPCMI, MPCMI, APCMI, and NAPCMI in the CNN model. NAPCMI-based features achieved the highest accuracy (97.76%), significantly outperforming the other methods. APCMI-based features also demonstrated strong performance, with an accuracy of 96.26%. In contrast, NPCMI- and PCMI-based features yielded lower accuracies of 93% and 91%, respectively.

Table 12. Average evaluation index of Delta-Gamma for brain-controlled plane group.

Feature Extraction Methods	Precision	Recall	F1-Score	AUC
PCMI	91.09%	91.09%	91.09%	0.969
NPCMI	92.75%	92.75%	92.75%	0.977
MPCMI	93.28%	93.28%	93.28%	0.978
APCMI	96.26%	96.26%	96.26%	0.990
NAPCMI	97.76%	97.76%	97.76%	0.993

4.3. Analysis of Experimental Data

Behavioral data and EEG signal data were comprehensively analyzed to evaluate the effects of spatial cognition training:

- Behavioral Data: After training, task completion time was significantly reduced, and scores were significantly improved, indicating that spatial cognition training effectively enhanced the participants' spatial cognitive abilities.
- EEG Signal Data: Using NAPCMI feature extraction and CNN classification, significant changes in EEG features were observed after training. These changes aligned with improvements in behavioral data, further confirming the enhancement of spatial cognitive abilities.

5. Discussion and Conclusions

5.1. Feasibility and Effectiveness of NAPCMI

The NAPCMI algorithm proposed in this paper demonstrates significant advantages in characterizing spatial cognitive EEG signal features. Compared with traditional methods such as PCMI and NPCMI, NAPCMI enhances the capture of time series information and effectively characterizes amplitude features, leading to improved connectivity metrics of brain regions. This enables NAPCMI to achieve superior classification accuracy, underscoring the importance of amplitude features in EEG signal classification tasks.

In terms of frequency band optimization, NAPCMI shows flexibility and effectiveness. Notably, the Delta and Beta1 bands perform well in spatial cognition tasks, with the Delta-Theta-Alpha1-Beta1 combination achieving the best results in experiments involving the hand-controlled plane and brain-controlled car. These findings further validate NAPCMI's adaptability to frequency band selection.

Compared with traditional CSP and MI-based methods, NAPCMI effectively detects interaction delays in event sequences between brain regions, demonstrates strong robustness to signal noise, and preserves intrinsic timing patterns [20–22]. Additionally, multi-group experiments show that NAPCMI outperforms PCMI in validation accuracy, recall, F1 score, and AUC. Its stability across learning rates and experimental conditions highlights its generalization ability and efficient classification performance, making it suitable for diverse datasets and experimental scenarios [15,23].

In summary, the NAPCMI algorithm provides robust and reliable technical support for EEG signal analysis in spatial cognition, with strong potential for practical application.

5.2. NAPCMI Classification Performance

In this study, a feature extraction method for EEG signals based on NAPCMI was proposed, and an efficient classification model using CNN was constructed to assess spatial cognitive abilities. Experimental results demonstrate that NAPCMI achieves superior classification performance, with a classification accuracy of 99.3% in CNN models, significantly outperforming traditional methods such as PCMI. By combining amplitude features and temporal information, NAPCMI enhances feature discriminability and accelerates model convergence.

- Frequency Band Selection:

The Delta-Theta-Alpha1-Beta1-Beta2 combination yielded the best classification results, consistent with prior studies.

For example, Hernández-Pérez et al. highlighted the role of the Theta band in spatial information encoding [24], while Li et al. demonstrated the Delta band's importance in spatial cognitive networks [25].

Changes in the Alpha1 band before and after training and the strong performance of Beta1 and Beta2 bands further validate NAPCMI's applicability to spatial cognition tasks.

- Classification Metrics:

NAPCMI outperformed PCMI, NPCMI, and MPCMI in recall, F1 score, and AUC.

NAPCMI achieved a recall rate of 99.35% and an AUC of 0.995, surpassing PCMI's 0.990 and APCMI's 0.994, demonstrating its superior ability to distinguish brain region activity patterns.

- Robustness and Stability

NAPCMI showed better robustness under high-noise conditions, consistent with findings by Siaw-Hong Liew et al. [26].

The algorithm achieved high accuracy and low loss values with fewer iterations, highlighting advantages in learning efficiency and adaptability across datasets and experimental conditions.

- Contributions and Future Work:

This study establishes NAPCMI as a robust tool for EEG signal classification and spatial cognitive assessment. By leveraging CNNs, we effectively evaluated changes in spatial cognitive abilities before and after training. Additionally, the proposed method holds potential for applications in cognitive impairment diagnosis, rehabilitation monitoring, and broader cognitive function assessments.

Future research will focus on validating NAPCMI on larger datasets and diverse scenarios, including cross-scene and cross-subject applications. Exploring additional EEG features and machine learning algorithms will further enhance classification accuracy and robustness, expanding the practical applicability of this approach.

Author Contributions: Conceptualization, X.W. and D.W.; Data curation, Z.W.; Funding acquisition, X.W. and D.W.; Investigation, Y.S. and Z.W.; Methodology, X.W. and Y.S.; Project administration, X.W. and D.W.; Supervision, D.W.; Validation, Z.W.; Visualization, Y.S. and Z.W.; Writing—original draft, X.W. and Y.S.; Writing—review and editing, X.W., Y.S., Z.W. and D.W. All authors have read and agreed to the published version of the manuscript.

Funding: This research was funded in part by National Natural Science Foundation of China (62206014 and 62276022), and in part by National Key Research and Development Program of China (2023YFF1203702).

Institutional Review Board Statement: The study was conducted in accordance with the Declaration of Helsinki, and approved by the Ethics Committee of the First People's Hospital of Qinhuangdao, Hebei Province (protocol code 2018B006 and date of approval is 6 March 2018).

Informed Consent Statement: Informed consent for participation was obtained from all subjects involved in the study.

Data Availability Statement: The datasets presented in this article are not readily available due to restrictions related to ongoing analyses and further research development. For any inquiries, please contact the corresponding author.

Conflicts of Interest: The authors declared no potential conflicts of interest with respect to the research, authorship, and publication of this article.

References

1. Xuqun, Y.; Bihua, Y. Cognitive processing characteristics of visuospatial ability. *J. Shaanxi Norm. Univ. (Philos. Soc. Sci. Ed.)* **2004**, *33*, 102–107.
2. Vidal, J.J. Toward direct brain-computer communication. *Annu. Rev. Biophys. Bioeng.* **1973**, *2*, 157–180. [CrossRef] [PubMed]
3. Morris, R. Developments of a water-maze procedure for studying spatial learning in the rat. *J. Neurosci. Methods* **1984**, *11*, 47–60. [CrossRef] [PubMed]
4. Song, S.; Zhang, Y.; Yuan, S. An experiment on urban spatial cognition based on virtual reality technology. In Proceedings of the 2013 National Architectural Digital Technology Teaching Seminar for Architectural Faculties and International Symposium on Digital Architectural Design, Tianjin, China; 2013; pp. 239–243.
5. Zhao, Z.; Wang, X.; Shen, L. Effect of cognitive function training on rehabilitation of patients with cognitive impairment after stroke. *China Pharm. Ind.* **2020**, *29*, 106–107. (In Chinese)
6. Rizzo, A.A.; Schultheis, M.; Kerns, K.A.; Mateer, C. Analysis of assets for virtual reality applications in neuropsychology. *Neuropsychol. Rehabil.* **2004**, *14*, 207–239. [CrossRef]
7. Shen, T.; Lin, H.; Liu, W.; Ge, H. Research progress of virtual reality technology applied to critically ill patients. *J. Nurse Adv.* **2022**, *37*, 416–419.
8. Mirelman, A.; Rochester, L.; Maidan, I.; Del Din, S.; Alcock, L.; Nieuwhof, F.; Rikkert, M.O.; Bloem, B.R.; Pelosin, E.; Avanzino, L.; et al. Addition of a non-immersive virtual reality component to treadmill training to reduce fall risk in older adults (V-TIME): A randomised controlled trial. *Lancet* **2016**, *388*, 1170–1182. [CrossRef] [PubMed]
9. Keskin, M.; Ooms, K.; Dogru, A.O.; De Maeyer, P. EEG & eye tracking user experiments for spatial memory task on maps. *ISPRS Int. J. Geo-Inf.* **2019**, *8*, 546. [CrossRef]
10. Zhao, J.; Song, J.; Li, X.; Kang, J. A study on EEG feature extraction and classification in autistic children based on singular spectrum analysis method. *Brain Behav.* **2020**, *10*, e01721. [CrossRef] [PubMed]
11. Martínez-Briones, B.J.; Bosch-Bayard, J.; Biscay-Lirio, R.J.; Silva-Pereyra, J.; Albarrán-Cárdenas, L.; Fernández, T. Effects of neurofeedback on the working memory of children with learning disorders—An EEG power-spectrum analysis. *Brain Sci.* **2021**, *11*, 957. [CrossRef] [PubMed]
12. Gu, Z.; Yan, G.; Zhang, J.; Li, Y.; Yu, Z.L. Automatic epilepsy detection based on wavelets constructed from data. *IEEE Access* **2018**, *6*, 53133–53140. [CrossRef]
13. Alturki, F.A.; AlSharabi, K.; Abdurraqeeb, A.M.; Aljalal, M. EEG signal analysis for diagnosing neurological disorders using discrete wavelet transform and intelligent techniques. *Sensors* **2020**, *20*, 2505. [CrossRef] [PubMed]
14. Li, H.; Feng, S.; Ma, L.; Xu, Z.; Xu, R.; Jung, T.-P. Common cross-spectral patterns of electroencephalography for reliable cognitive task identification. *IEEE Access* **2020**, *8*, 17652–17662. [CrossRef]
15. Li, X.; Ouyang, G. Estimating coupling direction between neuronal populations with permutation conditional mutual information. *NeuroImage* **2010**, *52*, 497–507. [CrossRef] [PubMed]
16. Estevez, P.A.; Tesmer, M.; Perez, C.A.; Zurada, J.M. Normalized mutual information feature selection. *IEEE Trans. Neural Netw.* **2009**, *20*, 189–201. [CrossRef] [PubMed]
17. Fang, L.; Zhao, H.; Wang, P.; Yu, M.; Yan, J.; Cheng, W.; Chen, P. Feature selection method based on mutual information and class separability for dimension reduction in multidimensional time series for clinical data. *Biomed. Signal Process. Control.* **2015**, *21*, 82–89. [CrossRef]
18. Das, S.N.; Mathew, M.; Vijayaraghavan, P.K. An approach for optimal feature subset selection using a new term weighting scheme and mutual information. In Proceedings of the International Conference on Advanced Science, Engineering and Information Technology, Kuala Lumpu, Malaysia, 14–15 January 2011; pp. 273–278.
19. Wu, C.-T.; Huang, H.-C.; Huang, S.; Chen, I.-M.; Liao, S.-C.; Chen, C.-K.; Lin, C.; Lee, S.-H.; Chen, M.-H.; Tsai, C.-F.; et al. Resting-state EEG signal for major depressive disorder detection: A systematic validation on a large and diverse dataset. *Biosensors* **2021**, *11*, 499. [CrossRef]
20. Hassan, K.M.; Islam, R.; Nguyen, T.T.; Molla, K.I. Epileptic seizure detection in EEG using mutual information-based best individual feature selection. *Expert. Syst. Appl.* **2022**, *193*, 116414. [CrossRef]
21. Li, J.; Liu, X.; Ouyang, G. Permutation conditional mutual information and its application to epileptic EEG. In Proceedings of the 2013 International Conference on Computer Sciences and Applications, IEEE, Washington, DC, USA, 14–15 December 2013; pp. 733–736.
22. Wen, D.; Bian, Z.; Li, Q.; Wang, L.; Lu, C.; Li, X. Resting-state EEG coupling analysis of amnestic mild cognitive impairment with type 2 diabetes mellitus by using permutation conditional mutual information. *Clin. Neurophysiol.* **2016**, *127*, 335–348. [CrossRef] [PubMed]

23. Li, Z.; Li, X. Causality of spike trains based on entropy. *Signal Process. Neurosci.* **2016**, 39–55.
24. Hernández-Pérez, J.J.; Gutiérrez-Guzmán, B.E.; López-Vázquez, M.; Olvera-Cortés, M.E. Supramammillary serotonin reduction alters place learning and concomitant hippocampal, septal, and supramammillar theta activity in a Morris water maze. *Front. Pharmacol.* **2015**, *6*, 250. [CrossRef] [PubMed]
25. Park, H.K.; Choi, S.H.; Kim, S.; Park, U.; Kang, S.W.; Jeong, J.H.; Moon, S.Y.; Hong, C.H.; Song, H.-S.; Chun, B.-O.; et al. Functional brain changes using electroencephalography after a 24-week multidomain intervention program to prevent dementia. *Front. Aging Neurosci.* **2022**, *14*, 892590. [CrossRef] [PubMed]
26. Liew, S.H.; Choo, Y.H.; Low, Y.F. Missing values imputation using similarity matching method for Brainprint authentication. *Int. J. Adv. Comput. Sci. Appl.* **2018**, *9*, 1044. [CrossRef]